Journal of Structural Geology, Vol. 11, No. 1/2, pp. 15 to 36, 1989
Printed in Great Britain

0191-8141/89 $03.00 + 0.00

Normal faulting in the upper continental crust: observations from regions of active extension

J. A. JACKSON and N. J. WHITE

Bullard Laboratories, Department of Earth Sciences, University of Cambridge, Madingley Road, Cambridge CB3 0EZ, U.K.

(*Received* 18 *February* 1988; *accepted* 3 *September* 1988)

Abstract—Observations of present-day normal faulting in regions of active continental extension may be helpful when interpreting the geological record in older extensional basins. The most obvious manifestation of active extension is normal faulting in earthquakes. Earthquake foci are mostly confined to the upper (seismogenic) continental crust, whose thickness imposes a scale on the observed deformation. Large earthquakes move faults with lengths similar or large compared with the thickness of the seismogenic layer. Large seismogenic normal faults on the continents appear to be restricted to a dip range of around 30–60°: dips significantly gentler than 20° have not been observed in fault plane solutions of large earthquakes. Large seismographic normal faults are approximately planar in cross-section and cut through the base of the upper seismogenic layer, rotating about a horizontal axis as they move. A reasonable estimate of the regional extension can often be made from the dip of the large normal faults and the tilt of the blocks they bound (the 'domino model'). Such faults are rarely continuous for more than 15–20 km, but commonly change strike or step in an en échelon fashion. This segmentation may occur on a scale controlled by the thickness of the seismogenic layer, and is an important influence on sedimentation and drainage.

These observations are common to large seismogenic normal faults from a variety of tectonic settings, and suggest that the kinematics of normal faulting may not be strongly influenced by the forces responsible for the extension, which can vary widely in nature and magnitude. Small earthquakes, which move faults that are small compared with the seismogenic layer thickness, show no simple pattern and often can be interpreted as internal deformation of blocks bounded by large faults.

In some places the seismogenic basement faults do not reach the surface but are decoupled from the sedimentary cover by layers of weak lithology. Faults in the sedimentary cover may be strongly curved in cross-section, requiring their hangingwalls to deform internally. Estimating extension from such faults is not straightforward and requires a knowledge of the hangingwall deformation. Estimates made in this way are often very non-unique and prone to large errors.

We postulate that the thickness of the seismogenic upper crust controls both the maximum length of large normal fault segments along strike and the maximum size of blocks that can rotate coherently about a horizontal axis.

INTRODUCTION

MANY continental sedimentary basins and passive margins are known to have formed as a result of crustal and lithospheric extension. At shallow levels, extension is manifest by normal faulting, and there has been considerable interest in trying to reconcile the amount of extension inferred from the faulting with that estimated for the crust or lithosphere as a whole from observations of crustal thickness, heat flow, or subsidence. In some areas, such as the North Sea (Ziegler 1983, Barton & Wood 1984) and Bay of Biscay (de Charpal *et al.* 1978, Le Pichon & Sibuet 1981) there is disagreement about whether extension of the upper crust is less than that of the crust (or lithosphere) as a whole. Elsewhere, such as in parts of the Basin and Range Province (Gans 1987), extension of the upper crust apparently exceeded extension of the crust as a whole: here, and on some stretched continental margins (e.g. White *et al.* 1987) the crust may not have been conserved during extension, but had magma added to it as a result of melting caused by asthenospheric upwelling and decompression (McKenzie & Bickle 1988). In all cases, it is important to have confidence that any apparent discrepancy between extension of the upper crust and the crust as a whole is real: and this requires an understanding of how extension is accommodated by normal faulting. Many recent papers have addressed this subject, usually concentrating on observations from inactive geological structures exposed at the surface or imaged on seismic reflection profiles. This paper explores a different source of information: observations of active normal faulting in continental regions undergoing extension today. These regions include Greece, western Turkey, Italy, the Gulf of Suez, Tibet, Yunnan, Mongolia, the Lake Baykal region, parts of NE China, the western U.S.A. and East Africa. All are seismically active and experience large normal faulting earthquakes. Seismological and surface observations of the faulting in these earthquakes provide information on the three-dimensional geometry of the extensional deformation at the time it is active. This information is summarized in the next section, before discussion of its significance for the understanding of regional crustal extension.

SEISMICALLY ACTIVE NORMAL FAULTING

Scale: the seismic–aseismic transition

Earthquake focal depths are not uniformly distributed throughout the continental crust, but are over-

whelmingly concentrated in the upper 10–15 km, with the lower continental crust remaining aseismic. This pattern is clear in high-quality locations from dense local seismograph networks (capable of ±1 km depth resolution) or in focal depths determined from seismic waveform modelling (capable of ±2 km or better in the best circumstances, e.g. Nabalek in press). The pattern is not clear in locations produced routinely using arrival time data from world-wide seismic stations (e.g. by the United States Geological Survey or by the International Seismological Centre), which can be in error by up to 50 km in focal depth. The observations supporting these statements are summarized by Meissner & Strehlau (1982), Sibson (1982), Chen & Molnar (1983) and Strehlau (1986). There are very few exceptions to this general pattern of focal depths, particularly among large earthquakes: four were reported by Shudofsky (1985) at depths of 25–30 km in East Africa, and a survey of the current literature (Appendix) shows that of 63 continental normal faulting earthquakes whose focal depths were determined by waveform modelling only four had depths greater than 17 km (the deepest being 29 km), and three of these were in East Africa. It is noteworthy that the elastic thickness of the lithosphere in East Africa may be as much as 25 km (Bechtel *et al.* 1987), which is greater than appears to be typical of other extensional regions (Bechtel & Forsyth 1987, Watts 1988; see later). Some earthquakes are also thought to occur in the uppermost mantle beneath the continental crust, though these are rare and apparently confined to places where the upper crust is also seismically active (e.g. Chen & Molnar 1983, Nelson *et al.* 1987).

Thus, in general terms, the continental crust consists of an upper layer in which earthquake hypocentres occur over a lower one that is aseismic. The thickness of the seismogenic layer is usually around 10–15 km and imposes a length scale on the geometry of deformation in the crust: in particular, faults have lengths that are either small, similar or large compared with the layer thickness. In the case of earthquakes, an event of magnitude ($\mathbf{m}_b$) 5.5 will have a fault length of about 10–15 km, whereas one of $\mathbf{m}_b$ 4.0 will involve a fault length of only about 100 m. Earthquakes larger than magnitude ($\mathbf{M}_s$) 6.5 involve faulting with a length (along strike) considerably greater than the thickness of the seismogenic layer. This distinction between 'large' and 'small' (compared with the seismogenic layer) faults (and earthquakes) has concerned seismologists for some time (e.g. Scholz 1982, Shimazaki 1986), but is probably less well known among structural geologists. It will concern us throughout this paper.

What is the nature of the seismic–aseismic transition in the crust? The seismicity cutoff with depth is probably temperature controlled, occurring in the region of 350 ± 100°C, and in simplest terms is thought to represent a change from pressure-sensitive frictional slip (not necessarily 'brittle': see Scholz 1988) at shallow levels to pressure-insensitive plastic flow at depth (see e.g. Meissner & Strehlau 1982, Sibson 1982, Chen & Molnar 1983). In reality, because the crust is a multi-mineralic material, the change in deformation mechanism within the shear zone is likely to occur over a depth interval, starting with the onset of plasticity of the most ductile component and ending with the full plasticity of the most brittle component (Scholz 1988). Within this transitional interval, sometimes called the 'semi-brittle' field, a mixture of brittle and plastic processes must occur (see e.g. Hobbs *et al.* 1986, Rutter 1986, Strehlau 1986, Scholz 1988). Scholz (1988) suggests that for a quartzofeldspathic material, the semi-brittle field occupies the region of about 300–450°C.

An important additional observation is that the focal depths of large earthquakes, obtained from waveform modelling, occur near the base of the seismogenic layer defined by the cutoff depth of microseismicity or aftershocks (Eyidoğan & Jackson 1985, Strehlau 1986). These focal depths are usually determined from long-period waveforms that have been generated over a finite fault area and represent an average depth of the radiating source: in other words they give the depth of a conceptual point source that produces the same seismic radiation as a much larger fault plane. The physical meaning of such focal depths is not straightforward. The higher the frequency of the waveforms the closer the 'focal depth' will be to the nucleation depth of rupture in the earthquake. At longer wavelengths the 'focal depth' will approach an 'average depth' of the radiating fault plane, which in the case of faults that rupture to the surface may be only half the actual depth extent of faulting. For the purposes of this paper the significance of the focal depths of large earthquakes being near the base of the seismogenic layer is that they almost certainly involve rupture as deep as the base of the seismogenic layer and probably continue to rupture downwards into the semi-brittle field (see Das 1982, Eyidoğan & Jackson 1985, Hobbs *et al.* 1986, Tse & Rice 1986, Scholz 1988).

In conclusion: (i) the continental crust consists of an upper seismogenic layer over an aseismic lower crust; (ii) within the upper seismogenic crust, the deformation in fault or shear zones is probably dominated by frictional processes. Below this, there is a transitional or semi-brittle field where both frictional and plastic processes occur. At greater depths plastic processes dominate the deformation; (iii) the seismogenic layer imposes a length scale on the crustal deformation: faults are either small, similar or large compared with its thickness; (iv) faulting in 'large' earthquakes ruptures down through the seismogenic layer into the transitional (semi-brittle) region, and often (though not always: for reasons discussed later) to the Earth's surface. Large earthquakes therefore involve faulting at depths that would usually be designated 'basement'.

Fault dips

Fault plane solutions of earthquakes provide information on the orientation of the seismic faulting. Reliable fault plane solutions for large earthquakes have been

obtainable since about 1962 using first motion polarities read on the long period instruments of the World Wide Standard Seismograph Network (WWSSN). These instruments have a good high frequency response and impulsive P wave onsets are often seen for large earthquakes. Fault plane solutions constructed from the polarities of impulsive onsets probably represent the orientation of the fault surface near the point of rupture initiation; though the less impulsive the onset the more the solution is likely to represent an 'average' fault orientation. For small earthquakes, whose polarities are read on short period instruments, the distinction is insignificant as the radiating fault is so small. Fault plane solutions of large normal faulting earthquakes (those with fault lengths similar or greater than the thickness of the seismogenic upper crust) on the continents show a very clear pattern (Fig. 1). Either of the two nodal planes in a fault plane solution could be the actual fault plane, so Fig. 1(a) includes both nodal planes. Fault plane solutions for 125 large normal faulting earthquakes that occurred in the period 1962–1987 and two from 1954 form the dataset in Fig. 1(a). Details of the earthquakes and references to their fault plane solutions are given in the Appendix. Dip errors are discussed by Jackson (1987) and are in the range 10–15° for most of the sample: solutions with uncertainties significantly greater than this have been excluded. Figure 1(b) is a subset of Fig. 1(a) and includes only those with a slip vector less than 30° either side of the down-dip direction. Again, both nodal planes are included for each earthquake. Those in black have been drawn with as gentle a dip as possible, and could be steeper (see Jackson 1987). Figure 1(c) includes only nodal planes that could be positively identified as the fault plane (usually by surface faulting).

It is clear from Fig. 1, and especially from Fig. 1(b), that the most common dip of nodal planes, regardless of whether they are the actual fault planes, is in the range 30–60°. The absence of dips significantly less than 20° or greater than 70° is particularly striking and is well constrained by the observations. Very low-angle (<20° dip) normal faulting requires a very steep (auxiliary) plane to pass through the central part of the focal sphere. This is the region best sampled by teleseismic data. In almost all the earthquakes shown in Fig. 1 dilatational first motions dominate the teleseismic distance range (30–80°), excluding the possibility of a very steep nodal plane, and thereby also excluding a very low-angle nodal plane.

First motion fault plane solutions can be combined with other observations, such as surface slip vector measurement, accurate epicentral position, focal depth or geodetic levelling, to constrain the shape of the fault in cross-section. In the few cases (five or six) for which these additional data have been of sufficient quality, the large normal faults appear to be roughly planar from the surface to the base of the seismogenic upper crust (Eyidoğan & Jackson 1985, Stein & Barrientos 1985, Barrientos *et al.* 1987, Nabalek in press), though the observations are rarely able to exclude a minor change in dip (up to 15°) between the surface and the hypocentre.

Fault plane solutions of small earthquakes in regions

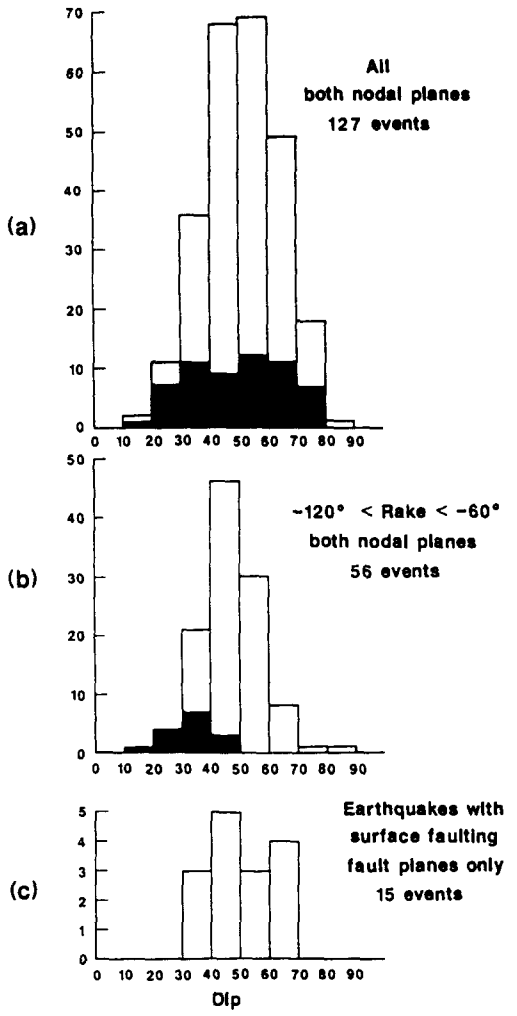

Fig. 1. Dips of nodal planes for large ($m_b \geq 5.2$) continental normal faulting earthquakes, measured from fault plane solutions. This figure includes data from Greece, western Turkey, Italy, the Gulf of Suez, Tibet, NE China, SW China, Mongolia, East Africa, and the western U.S.A. The black region in (a) includes dips from moment tensor inversions carried out at Harvard (the method of Dziewonski & Woodhouse 1983), and published by the United States Geological Survey. The black region in (b) includes dips that have been deliberately drawn to be as gentle as possible (i.e. minimizing the strike-slip component): they could be steeper.

of active extension show no simple pattern. This is best illustrated by detailed high-quality studies of aftershock sequences, where normal faulting mainshocks may be followed by aftershocks of almost any orientation and mechanism, including reverse faulting (e.g. Deschamps & King 1984, Richens *et al.* 1987, Westaway & Jackson 1987, Lyon-Caen *et al.* in press). Most aftershocks do not occur on the mainshock fault plane and appear to represent internal deformation of the blocks bounded by large faults. Although very numerous, the small aftershocks can often be shown to account for much less cumulative deformation than the movement in the mainshock (e.g. Westaway & Jackson 1987).

Vertical movements and tilting

Both tilting and vertical movements are observed to accompany slip on active normal faults. Vertical movements involve uplift of the footwall and subsidence of

the hangingwall blocks and can be observed either geodetically (Jankhof 1945, Richter 1958, Myers & Hamilton 1964, Savage & Hastie 1966, Stein & Barrientos 1985, Barrientos *et al.* 1987) or by reference to sea level (Jackson *et al.* 1982a). These vertical movements decrease with distance from the fault and thus cause a tilting of the footwall and hangingwall blocks. The fault consequently rotates about a horizontal axis, reducing its dip. These observations may be interpreted in several ways that are not mutually exclusive. The vertical movements adjacent to a single normal fault may be seen as either the effect of elastic rebound immediately following fault slip (e.g. Savage & Hastie 1966, Stein & Barrientos 1985), or, in the longer term, as an isostatic and flexural response to unloading of the footwall (Jackson & McKenzie 1983). However, normal faults rarely occur in isolation, but are commonly distributed across zones in which several subparallel faults dip in the same direction. Thus a single block is likely to be both the footwall of one fault and the hangingwall of another. The forces imposed on the block as a result of slip on its bounding faults represent a torque requiring the block to rotate about a horizontal axis, so as to reduce the dip of the faults. This is the familiar 'rotating domino' style of extension (Ransome *et al.* 1910), and will be discussed later. It can be considered as the achievement of overall pure shear (crustal thinning and extension) by simple shear (faulting) and rotation (see Jackson 1987).

The observation that large normal faults tend to decrease their dip as they move suggests an explanation for the range of nodal plane dips shown in Fig. 1: that such faults start to move at dips no steeper than about 60° and rotate until they reach a dip of about 30° (Jackson 1987). This range is, to some extent, predicted by an analysis of fault mechanics following the principles of Anderson (1951) and Sibson (1985), which is discussed by Jackson (1987).

Continuity along strike

The largest known normal faulting earthquakes on the continents are far smaller than the largest thrust or strike-slip events. Particularly in Asia, several examples are known of thrust and strike-slip earthquakes with magnitude (M_w) greater than 8.0 or seismic moment (M_o) greater than 10^{21} Nm. These events involve fault lengths which exceed 100 km (e.g. Seeber & Armbruster 1981, Molnar & Deng 1984). (M_o is defined as the product $\mu A\bar{u}$, where μ is the rigidity modulus, A is the

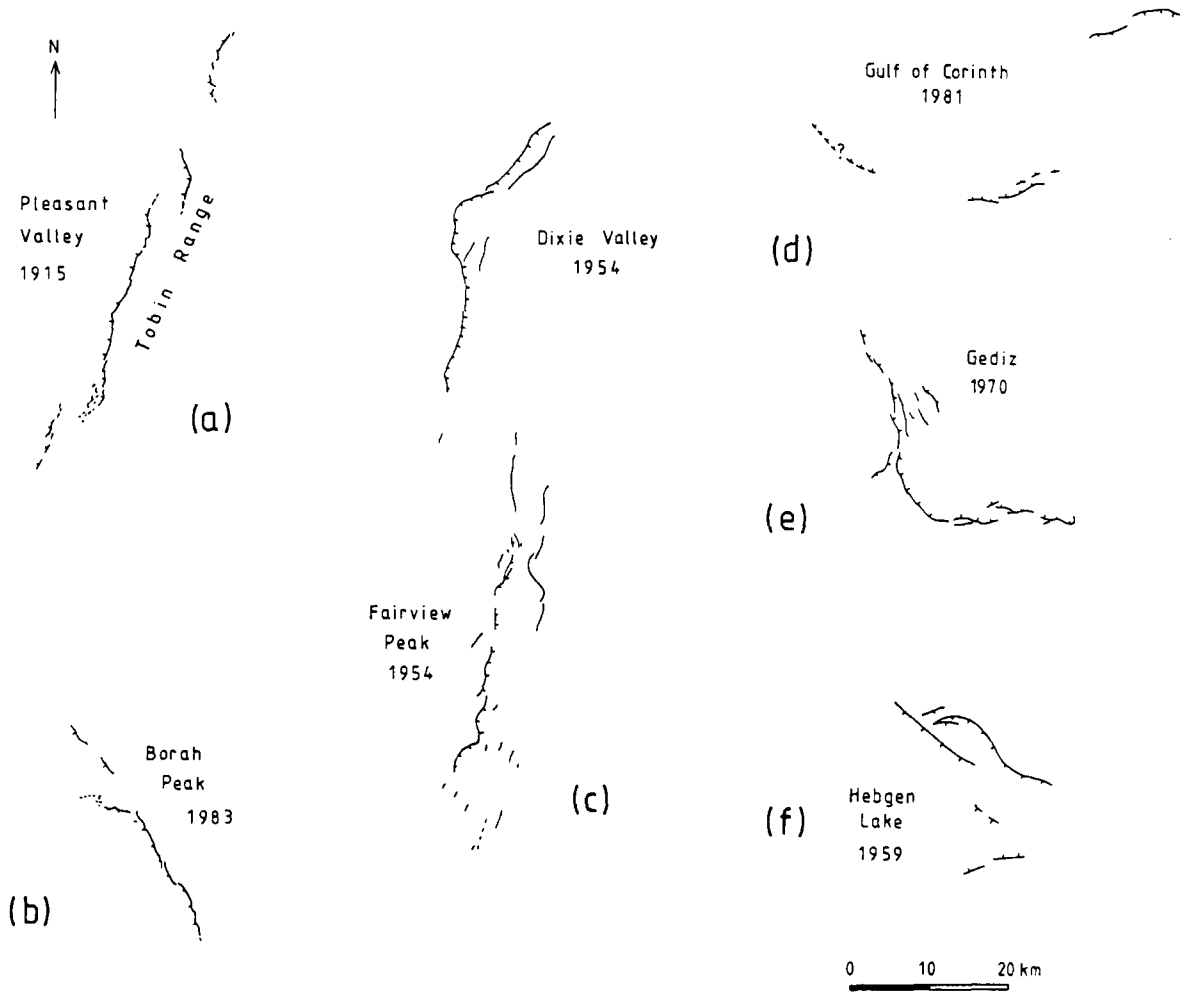

Fig. 2. Maps of the surface faulting observed in some large continental normal faulting earthquakes, all drawn to the same scale. Summarized from: Romney (1957), Fraser *et al.* (1964), Ambraseys & Tchalenko (1972), Jackson *et al.* (1982a,b), Crone & Machette (1984) and Wallace (1984).

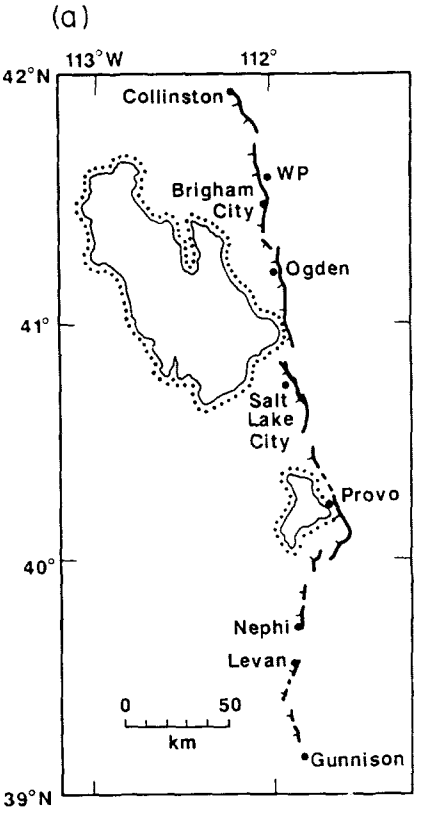

(b)

Fig. 3. (a) Summary map of the Wasatch Fault zone, Utah, after Schwarz & Coppersmith (1984). (b) View south along the Wasatch Front, taken from Willard Peak, (WP in a), north of Brigham City.

area of the fault plane and $\bar{u}$ is the average slip.) Only three normal faulting earthquakes are known that may have had moments as large as 10^{20} Nm: the 1915 Pleasant Valley, Nevada (Wallace 1984; $M_o \sim 0.7 \times 10^{20}$ Nm), the 1957 Muyu, Siberia (Molnar & Deng 1984; $M_o \sim 1.0 \times 10^{20}$ Nm and the 1959 Hebgen Lake, Montana (Doser 1985, Barrientos *et al.* 1987; $M_o \sim 1.0 \times 10^{20}$ Nm) earthquakes. The total lengths of faulting in these earthquakes were about 60, 40 and 35 km, respectively. However, in no large normal faulting earthquake has the faulting been continuous along strike for more than about 25 km (Fig. 2). The largest events commonly involve faulting in segments of up to about 20 km in length, which are either arranged en échelon or separated by gaps, or involve a dramatic change in strike along the length of the rupture zone. Such segmentation is often reflected in the geomorphology of the associated fault scarps, suggesting that the faults had moved in a similar segmented fashion before. Segmentation of major fault zones has been of interest to seismologists for some time, as discontinuities along the length of the fault appear to control the initiation and halting of rupture in earthquakes (e.g. Aki 1979, Lindh & Boore 1981, King & Nabalek 1985). Quite minor changes of strike, such as 5° in the 1966 Parkfield strike-slip earthquake (cf. the small change in strike midway along the central long segment of the 1915 Pleasant Valley faulting in Fig. 2a), may strongly influence rupture initiation and propagation. Seismograms from earthquakes exhibiting discontinuous surface faulting often show that slip occurred in discrete 'sub-events' separated by a few seconds (e.g. Doser 1985, Eyidoğan & Jackson 1985, Yielding 1985), indicating that the surface segmentation extends to depth. Segmentation of active fault systems can also be recognized in the geology, geomorphology and movement history of young fault scarps (revealed by trenching) where no historic earthquakes are known. An example is the Wasatch Front in Utah, which is an active normal fault system that is over 300 km long and clearly segmented along strike (Swan *et al.* 1980, Schwarz & Coppersmith 1984). Although early work on the Wasatch Front suggested that individual segments may be as long as 60 km (Schwarz & Coppersmith 1984), more recent investigations indicate that the segment lengths are probably much smaller (Machette *et al.* 1986, Bruhn *et al.* 1987). The Wasatch Front is a particularly good example of a large normal fault system with salients and embayments in plan view that would be expected to influence the lateral extent of rupture propagation in earthquakes. The salients are dramatic geomorphological features, disrupting the continuity of the hangingwall along strike (Fig. 3), and allowing the intervening embayments to develop as almost independent faults with varying throws and different sediment thicknesses in their hangingwalls (Schwarz & Coppersmith 1984).

Fault segmentation is not only of interest in earthquake mechanics, it strongly influences sedimentation in regions of active normal faulting. For example, drainage that flows off the back of uplifted and tilted footwall blocks and then longitudinally (along strike), may escape into the hangingwall of the graben where the fault segment (and hence topography and uplift) die out along strike. Thus major outwash fans may be located in specific positions along a graben axis, controlled by the segmentation of the bounding faults. In these circumstances, the influences of structure on sedimentation is very three-dimensional and not limited to material washing off the fault scarp perpendicular to strike. Leeder & Gawthorpe (1987, fig. 4) illustrate this sort of sedimentary environment, of which a good modern example is the south side of the Gulf of Corinth in Greece. If the pattern of segmentation seen in active normal faults today applies to older extensional basins, the faults bounding long graben systems may not be as continuous as they at first look (perhaps through insufficiently dense seismic reflection coverage). Major outwash fans may then be expected to occur where fault segments die out or change strike. The location of some of the major sediment fans in the South Viking Graben of the North Sea (Stoker & Brown 1986) may be an example of this phenomenon (Fig. 4). Finally, we note that in some of the subhorizontally outcropping faults or shear zones exposed in the Metamorphic Core Complexes of the western U.S.A., large-scale corrugations of faults and mylonitic foliation surfaces are observed with axes parallel to the direction of transport (Spencer & Reynolds in press). The corrugations are particularly well developed in the Buckskin–Rawhide–Harcuvar mountains of N.W. Arizona, where they have a wavelength of 15–20 km; similar to the maximum segment length we observe for active normal faults. The corrugations might be the deeper expression of the embayments and segmentation seen at the same scale on steeper active normal faults.

In conclusion, we are unaware of surface normal faulting in large earthquakes that is continuous, in the sense of lacking lateral offsets or changes in strike, for more than about 20 km; and most is less continuous than that. A similar segmentation length is seen in detailed maps of many active graben systems (e.g. Moore 1960, Myers & Hamilton 1964, Garfunkel & Bartov 1977, Allen *et al.* 1984, Armijo *et al.* 1986).

There is little doubt that faults are also segmented on a scale much smaller than this; of interest here is whether there is a *maximum* segment length for large normal faults. Although the evidence currently available is limited, we think it suggests that maximum segment lengths of about 20 km are very common.

Faulting in the lower crust?

As discussed earlier, the upper seismogenic crust is likely to be separated from the fully plastic lower crust by a transition zone of finite width in which both brittle and plastic processes can occur. It has been suggested that during large earthquakes rupture can propagate down into this 'semi-brittle' field (e.g. Das 1982, Eyidoğan & Jackson 1985, Hobbs *et al.* 1986, Strehlau 1986, Tse & Rice 1986, Scholz 1988). One reason for this is the

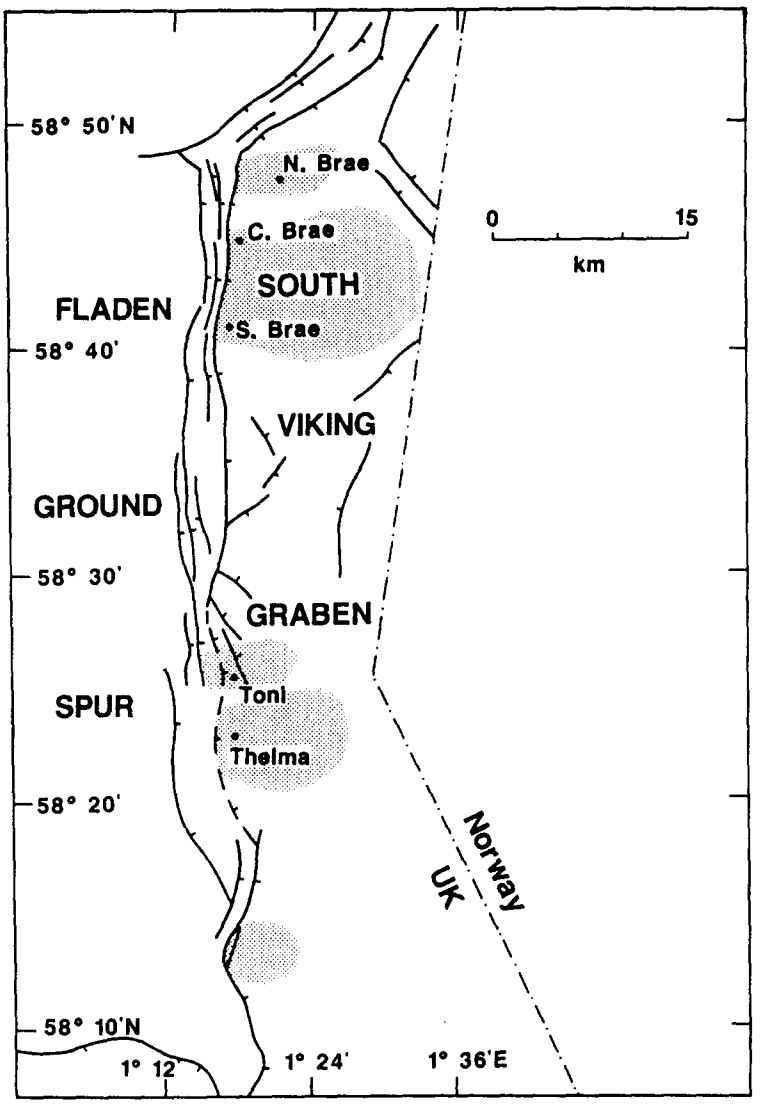

Fig. 4. Generalized interpretive map of the South Viking Graben, showing the major faults in the U.K. sector, the distribution of clastic sediment fans (stippled) and oilfields (after Stoker & Brown 1986).

enormous increase (8–10 orders of magnitude) in strain rate experienced by the top of the transition zone as fault rupture impinges on it from above. Under these conditions, material that would normally deform plastically at the ambient temperature will fail brittlely instead. The deformation in the transition zone could thus be brittle (during large earthquakes) or plastic (in between large earthquakes) depending on the strain rate. This dual behaviour is probably responsible for the intermixed and reworked mylonites and pseudotachylites described by Sibson (1980) and Hobbs *et al.* (1986), among others.

It is not certain how far rupture propagates beneath the seismogenic layer. Some large normal faulting earthquakes contain signals in the later part of their long period seismograms that may be interpreted as radiation from a relatively flat (dip of 20° or less) fault beneath a steeper fault in the upper crust: suggesting that as a rupture enters the transition zone it decreases its dip (Eyidoğan & Jackson 1985, Westaway & Jackson 1987). Because they are late in the seismogram, these signals are difficult to model and their interpretation is ambiguous. Other large normal faulting earthquakes contain no such signals and show no evidence that the fault flattens in the transition zone (Nabalek in press).

Below the depth of earthquake rupture penetration it is unclear how much deformation is concentrated on mylonitic shear zones that are downward continuations of higher level faults, and how much it is accommodated by more distributed flow; nor is it clear how this partitioning changes with depth. Detailed discussion of this issue is beyond the scope of this paper. Although some have argued for full crustal penetration of shear zones (Wernicke 1985), there is evidence in some places that the lower crust deforms by distributed flow. The best examples are from the Basin and Range province where both Gans (1987) and Spencer & Reynolds (in press) describe areas where substantial thinning of the crust beneath horst blocks has occurred. There is no obvious way in which this can be achieved by faulting, and lower crustal flow is more likely. The causes and consequences of such flow are discussed elsewhere (Kusznir & Matthews 1988, Gans *et al.* in prep.). Here it is sufficient to point out that there may be no justification for 'balancing' crustal-scale cross-sections (in the sense of

preserving cross-sectional area) by assuming rigid movement of fault bounded blocks at depths within the lower crust, where much of the deformation may have occurred by flow and not by faulting.

ESTIMATING EXTENSION FROM LARGE BASEMENT NORMAL FAULTS

The rotating domino model

Large normal faults in basement rocks tend to occur in zones containing several subparallel faults that dip the same way and rotate as they move to give the tilted terrains characteristic of many extended basins (e.g. Morton & Black 1975, Garfunkel & Bartov 1977, Stewart 1980). The 'rotating domino' model (e.g. Ransome *et al.* 1910, and subsequently many others) illustrates how this configuration can accommodate extension (Fig. 5). Such large normal faults are thought to be approximately planar and to rotate as they move: in good agreement with seismological observations. The virtue of the domino model is its extreme simplicity. Note that in Fig. 5 the faults do not extend to the Moho, which remains flat: this is the domino model on a crustal scale in its simplest form, in which we assume that the lower crust can flow. It is a common misconception that the bases or keels of the rotating blocks represent a space problem. On the scale of the faults shown in Fig. 5 this belief arises from a misunderstanding of the seismic–aseismic transition, which is likely to be a temperature horizon and so neither compositional nor fixed to the rotating blocks. Rotation of the blocks produces a perturbation to the initial temperature profile that will decay with a time constant of $L^2/4\pi^2\kappa$, where κ is the thermal diffusivity ($\sim 10^{-6}$ m s^{-1}) and L is the spacing of the faults (see Jackson *et al.* 1988). This time constant is very short, being only 0.5 Ma for faults 25 km apart. Unless all the extension occurs quickly compared with this time, the seismic–aseismic transition will not be perturbed significantly by the block movement. Figure 5 assumes the lower crust has deformed by flow: there is no need for a subhorizontal 'detachment' or 'décollement' zone of discrete slip at the base of the tilted blocks, and calculations of the depth to such a horizon are meaningless.

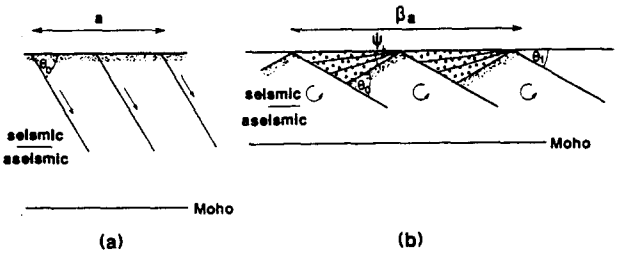

Fig. 5. Cartoon sections to illustrate the rotating block ('domino') style of extension. Faults start with a dip θ_0, then tilt through an angle ψ to attain a new dip θ_1. The surface area increases by a factor β. Sediments infilling the grabens (open circles) show growth towards the bounding faults. We do not show faults below the seismic–aseismic transition, which we show to be raised by the extension. Whether it is actually raised depends primarily on the extensional strain rate (see England & Jackson 1987).

The domino model allows an estimate of β, the amount of extension (defined in Fig. 5), from the initial (θ_0) and final (θ_1) fault dips, using the relation:

$$\beta \sin \theta_1 = \sin \theta_0 \qquad (1)$$

(see Le Pichon & Sibuet 1981, Jackson & McKenzie 1983). Note that the tilt is given by $\psi = \theta_0 - \theta_1$. Figure 1 suggests that, for large seismogenic normal faults, the maximum value of θ_0 is about 60–70° and the minimum value of θ_1 is about 30°. From equation (1) the maximum amount of extension (β_{max}) obtainable by simple domino-style rotation on planar faults restricted to this dip range is in the region of 1.7–2.0. Extension of up to this amount can therefore be accommodated by a single generation of rotating planar faults that are not required to move outside the dip range observed in Fig. 1. Extension greatly exceeding $\beta = 2$ requires something else to happen. One possibility is that a second generation of normal faults starts to move once the first generation has rotated to a dip of 30°. The second-generation faults cut the first generation making them inactive, and rotating them passively to still gentler dips. The total extension is then:

$$\beta_{total} = \beta_1 \times \beta_2 \times \ldots \times \beta_n, \qquad (2)$$

where β_n is the extension caused by the nth generation of normal faults. Several authors have suggested this mechanism in areas where extension exceeds $\beta = 2$, and where a syn- (or immediately pre-) faulting unconformity provides a horizontal reference level that can be restored and used to estimate the dip of the faults when they were active. In particular, Morton & Black (1975), Proffett (1977), Chamberlain (1983) and Gans & Miller (1983) all reported more than one generation of large rotating normal faults, but their observations did not require the faults to have been active significantly outside the dip range 30–60°; nor were the faults required to be significantly curved in cross-section. Their interpretations are obviously not in conflict with seismological observations of large active normal faults today.

There are several well-known difficulties with the domino model in its simplest form. It is not clear how to accommodate the differential rotation about a horizontal axis between a tilted extended terrain and its stable margin or a horst block (see e.g. Wernicke & Burchfiel 1982, Gans & Miller 1983). Moreover, the model requires all the faults to be simultaneously active across the whole basin with the same dip and the same tilt to their fault-bounded blocks, whereas in fact the timing, tilting and extension often varies across a basin (e.g. Morton & Black 1975, Gans & Miller 1983, Barton & Wood 1984, Gans 1987). Many of these difficulties can be resolved if the faults are not perfectly planar or if the blocks they bound are not perfectly rigid but deform internally by small-scale faulting, folding or flow. Such solutions may seem *ad hoc,* but are only being realistic about the uncertainty of the seismological (or geologi-

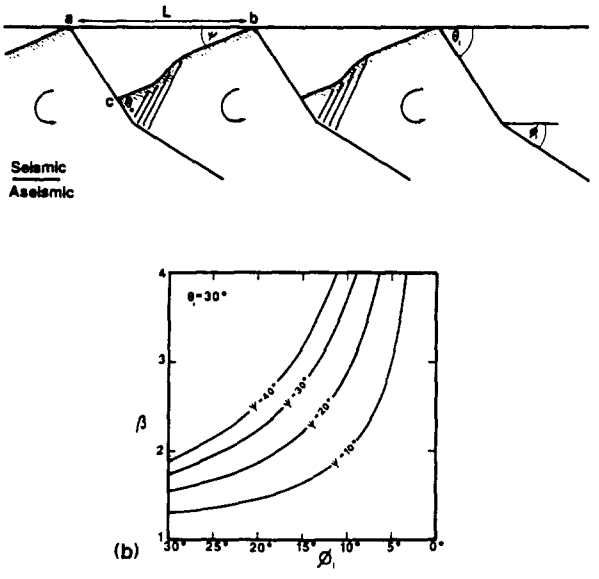

Fig. 6. The effect of fault curvature (a) on the amount of extension achieved by rotating faults (from White 1988). ψ is the amount of tilt and ϕ_1 the dip of the fault at depth. θ_0 and ϕ_0 were the initial dips of the fault at the surface and at depth. The example in (b) is for a fault whose final dip at the surface (θ_1) is 30°. Thus when $\phi_1 = 30°$ the fault is planar and $\beta = 1.5$ for $\psi = 20°$. If ϕ_1 decreases to 15° and ψ stays the same, then $\beta = 2.1$.

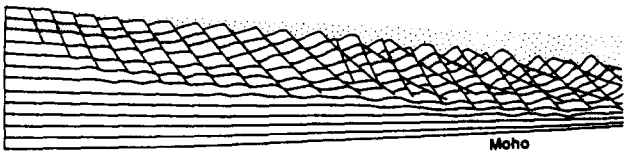

Fig. 7. Cartoon to show progressive crustal attenuation across a basin in which extension is accommodated at shallow levels by rotational block faulting and at deeper levels by flow (redrawn after Morton & Black 1975, and Chamberlain 1983). The stippled region represents post-stretching basin infill. Note how extension and tilt increase across the basin, and how internal deformation of the fault bounded blocks (particularly at depth) is able to take up differential tilting.

cal) observations: only very rarely can seismological data or techniques rule out a concave-up (listric) fault curvature of up to 10–15° (e.g. Nabalek in press), and the many aftershocks that follow large normal faulting earthquakes do not, in general, occur on the main seismogenic fault, but in the blocks either side; attesting to their internal deformation. It is possible to allow for fault curvature and the necessary accompanying internal deformation of the footwall or hangingwall blocks when estimating β from the fault dip and amount of rotation. Figure 6 shows the effect of fault curvature on the estimate of β, which is then given by:

$$\beta \sin \phi_1 = \sin \phi_0, \qquad (3)$$

where the tilt $\psi = \phi_0 - \phi_1$, ϕ_0 and ϕ_1 being the initial and final dips of the fault at depth. Perhaps surprisingly, the dip of the fault at the surface, θ_1 does not matter (White 1988). Note that fault curvature increases the extension for a given rotation (ψ) because the fault bounded blocks are not rigid. In other words, assuming that planar faults bound rigid blocks will tend to underestimate the amount of extension.

The usefulness of the simple domino model should be emphasized, while acknowledging that there are difficulties with it. It is simple, allows a quantitative estimate of β and can also be used to estimate quantitatively the vertical movements (both uplift and subsidence) that accompany block rotation and extension, and that control sedimentation (Barr 1987a,b, Jackson *et al.* 1988). Figure 7 is adapted from Morton & Black's (1975) cartoon illustrating progressive crustal attenuation across Afar, and though schematic, shows how tilting and fault complexity may increase as the centre of the basin is approached, and how differential rotation may be accommodated by some internal deformation of the fault-bounded blocks. The extension varies across the basin, but in each place may be estimated from equations (1) and (2). Note that if the blocks deform internally it will be difficult to 'balance' the section by simply restoring the major faults.

Although tilted domino-like terrains are common in some extended regions, others, which have fewer faults and are less extended, look different. In southern Tibet, for example, the major graben are separated by 100 km or more across strike (Armijo *et al.* 1986). It is improbable that blocks of this size rotate rigidly (see later). These grabens effectively occur in isolation. Footwall uplift and hangingwall subsidence are expected to occur as the isostatic forces following fault movement still apply (Jackson & McKenzie 1983), but will die out away from the fault at a distance dependent on the flexural strength of the surrounding material (Heiskanen & Vening Meinesz 1958).

Other mechanisms: very low-angle normal faulting

Work over the last decade in the Cordilleran Miogeocline and Metamorphic Core Complexes of the Basin and Range Province in the western U.S.A. has led to the suggestion that the crust can extend on large, planar, non-rotational normal faults that dip at a very low angle (0–20°) through the entire upper seismogenic crust (e.g. Wernicke 1981). As is clear from Fig. 1, this suggestion cannot be verified by looking at large seismogenic normal faults that are active today, nearly all of which dip in the range 30–60° and cut right through the upper seismogenic layer. There are no known examples of large earthquakes on subhorizontal normal faults on the continents. This dilemma may be resolved in a number of *ad hoc* ways, discussed by Jackson (1987), including: the proposal that very low-angle normal faults move aseismically (i.e. by creep); that they are spatially separated from high-angle normal faults (which would otherwise cut them); or that the sample period used for Fig. 1 (about 30 years) is not long enough. None of these explanations are really satisfactory. At issue here is whether the available geological observations are able to constrain the dips at which the apparently very low-angle faults were active: they are now inactive, the motion on most of them being Miocene or younger in age. This is a question that is best addressed by fieldwork. Although a

major issue in the current debate on extensional tectonics, it is not within the scope of this paper, which is to review information from active normal faulting.

FAULTS IN THE SEDIMENTARY COVER

Although large continental earthquakes involve faulting at depths that would normally be designated 'basement', faulting does not always rupture through to the surface. An example is the 1976 Luanxian earthquake in NE China, one of the largest recent normal faulting events ($M_o = 3 \times 10^{19}$ Nm) on the continents, which, based on the estimated rupture duration of 10 s (Nabalek *et al.* 1987), must have involved faulting with a total length of about 30 km, yet did not break the surface. Absence of surface faulting in large earthquakes is common where there is a thick sequence of sediments decoupled from the basement by one or more weak layers, such as overpressured shales or evaporites. This phenomenon occurs, for example, in the Zagros mountains of SW Iran (e.g. Jackson & Fitch 1981), where in spite of frequent large earthquakes on high-angle reverse faults in the basement, no faulting accompanying these earthquakes has been observed at the surface.

The decoupling of the deformation in the sedimentary cover from that in the basement is a well-known geological phenomenon, and can be seen, for example, in the Central Graben of the North Sea (e.g. Gibbs 1984). The pre-rifting sedimentary cover must extend the same amount as the underlying basement, but need not do so in the same style or even in precisely the same place. It should therefore be possible to estimate the amount of extension from structures in the cover, where, in particular, strongly curved (listric) normal faults are common, usually flattening onto weak layers at depth (illustrated schematically in Fig. 8). There is no evidence that such faults generate large earthquakes, and they presumably move aseismically. Faults of this sort require substantial internal deformation of their footwall or hangingwall blocks (e.g. Verrall 1981, Gibbs 1983, Davison 1986, White *et al.* 1986, Williams & Vann 1987). Detailed discussion of this topic is not appropriate here: we will simply summarize the points we regard as relevant to the calculation of extension from such structures.

(i) It is usually assumed that the footwall block remains rigid and only the hangingwall deforms internally in response to fault movement. Except where there is an obvious strength contrast between the two blocks, there is no real justification for this assumption; it simply makes a solution of the problem much easier. In the case of a dipping fault embedded in an elastic half-space, the free surface produces an asymmetry requiring the hangingwall to deform more than the footwall, which can be seen in all elastic solutions (see e.g. Stein & Barrientos 1985).

(ii) Knowledge of the hangingwall deformation is vital for an accurate estimate of the extension. Flexural slip has been suggested as a possible mechanism of hangingwall deformation (e.g. Davison 1986), but we believe that, because of antithetic faulting, compaction and sediment thickness variations, all of which are commonly observed within the hangingwall, penetrative simple shear is likely to be a better approximation (see White 1988). Simple shear may be inclined at any angle to the vertical and its inclination greatly affects the estimate of extension (White *et al.* 1986). Only if the simple shear is vertical is the extension equal to the apparent horizontal displacement across the fault. White (1987, 1988) argues that the shear is commonly inclined at about 45° towards the fault, in which case the true extension would be double the heave on the fault, if its dip changed from 45° at the surface to horizontal at depth.

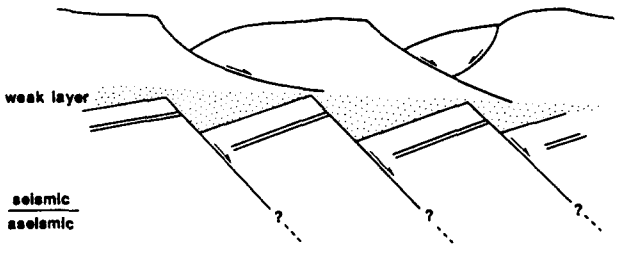

Fig. 8. Schematic cartoon to show how a lithologically weak layer (e.g. overpressured shale or salt) may allow the extension in the sedimentary cover to be decoupled from the fault-bounded tilted blocks in the basement below.

(iii) It will rarely be possible to know the style of internal deformation within the fault-bounded blocks with any confidence. If it is ignored, estimates of extension are likely to be too low (sometimes dramatically) rather than too high (White 1987, 1988). It is therefore difficult to estimate extension reliably from structures in the sedimentary cover.

DISCUSSION

Controls on the scale of normal faulting

(a) *The size of rotating blocks.* There appears to be an upper limit to the size of coherent blocks that can rotate about a horizontal axis. Tilted blocks are separated by normal faults about 20 km apart in the North Viking Graben of the North Sea (e.g. Ziegler 1982, Giltner 1987), by faults up to about 25 km apart in the Gulf of Suez (e.g. Jackson *et al.* 1988) and by faults as much as 30–40 km apart in the Basin and Range Province of the western U.S.A. (Fletcher & Hallett 1983). In central Greece major normal faults are separated by up to 40 km (Jackson & McKenzie 1983), but it is not clear whether the intervening blocks rotate coherently: they probably do not, because major faults dipping in both directions are common. Where the separation between half-graben is much larger than this, as in southern Tibet (Armijo *et al.* 1986), there is no evidence that the intervening blocks rotate coherently: the grabens appear to occur in effective isolation.

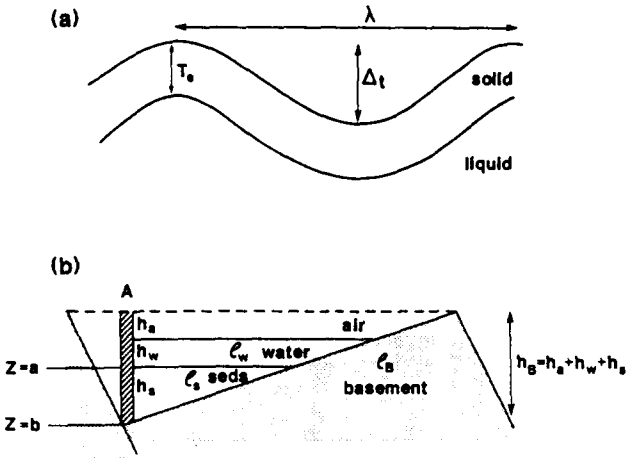

Fig. 9. (a) Deformation of a solid elastic layer of thickness (T_e) above a liquid of the same density (after McKenzie 1967). The deformation is exaggerated. (b) Cross-section illustrating the symbols used to calculate the effective basement topography when the graben is partly filled with sediments (thickness h_s) and water (thickness h_w).

What controls the upper size limit of rotating blocks? Because of the density contrast between the tilted basement blocks and the graben infill, stresses are necessary within the upper elastic layer in order to maintain the basement topography. If we assume that the situation shown in Fig. 5(b) is represented approximately by a solid elastic layer of thickness T_e overlying a liquid of the same density (the lower crust), we can calculate the maximum shear stress, σ_{max}, required to support the topography of the upper layer. The stress depends on the wavelength (λ) of the topography and the thickness of the elastic layer (Fig. 9a). Because the wavelengths of interest to us here are not large compared to πT_e, we cannot use the thin plate approximation (see e.g. McNutt 1980), but must use the full formulation of the problem, described by McKenzie (1967). If we rewrite equation (56) of McKenzie (1967), a sufficiently accurate solution for σ_{max} is:

$$\sigma_{max} = \frac{\rho_B g\, \Delta t}{2} H(k'), \tag{4}$$

where

$$H(k') = \begin{cases} 1/e & \text{if } k' > 2 \\ 3/4k' & \text{if } 1 < k' < 2 \\ 3/4k'^2 & \text{if } k' < 1 \end{cases}$$

and

$$k' = \pi T_e/\lambda. \tag{5}$$

Δt is the effective amplitude of the topography, ρ_B is the density of the basement (footwall), g is the acceleration due to gravity and k' is the dimensionless wavenumber (Fig. 9a). Figure 9(b) shows how to calculate the effective basement topography if the graben is partly filled with sediment and water. The mass (M_g) of the sedimentary and water column at the deepest point in the graben is given by

$$M_g = h_w \rho_w + \int_a^b \bar{\rho}_s \, dz, \tag{6}$$

where $\bar{\rho}_s$ is the average sediment density over a depth interval dz. The equivalent height (h_e) of a column of material with the same density as the basement, would be:

$$h_e = \frac{M_g}{\rho_B} \tag{7}$$

and the effective amplitude of the basement topography is

$$\Delta t = h_B - h_e \tag{8}$$

which may be substituted into equation (4).

We assume the graben sediments are able to compact, and that porosity ($\phi(z)$) varies with depth (z) in the form:

$$\phi(z) = \phi_0 \exp\left(\frac{-z}{l}\right), \tag{9}$$

where ϕ_0 is the initial porosity (at deposition) and l is the decay length (see e.g. Sclater & Christie 1980). The average sediment density $\bar{\rho}_s$ then varies with depth:

$$\bar{\rho}_s = \rho_s - (\rho_s - \rho_w)\phi(z), \tag{10}$$

where ρ_s is the density of the solid part of the sediment. Equation (7) then becomes:

$$M_g = h_w\rho_w + h_s\rho_s - \phi_0(\rho_s - \rho_w)l \times \left\{\exp\left(\frac{-a}{l}\right) - \exp\left(\frac{-b}{l}\right)\right\}, \tag{11}$$

where $z = a$ is the depth beneath the level at which $\phi = \phi_0$.

For a given layer thickness (T_e), equation (4) shows that, providing $k' < 2$, the stresses necessary to maintain the saw-tooth basement topography increase as the wavelength, density contrast and amplitude of the deformation increase. Because the effective basement topography decreases if the graben fills with sediment, the maximum stress correspondingly decreases. The general behaviour of equation (4) is illustrated in Fig. 10, which shows how the stresses supporting a saw-tooth basement topography depend on the amplitude and wavelength of the topography as well as on the density of the graben fill.

Table 1 illustrates the dependence of σ_{max} on λ and Δt for various extensional terrains. Following Wiens & Stein (1983), we assume that the thickness of the elastic layer is approximately the thickness of the seismogenic upper crust (we take T_e = 15 km), except in the case of the Viking Graben, where the elastic thickness is known to be much smaller (Barton & Wood 1984), and we take T_e = 5 km. Table 1 shows the expected increase in σ_{max} as λ increases. For the examples from the Gulf of Suez, Nevada, Greece and Tibet, where we have taken T_e = 15 km, once $\lambda > 47$ km then $k' < 1$ and, because $\sigma_{max} \propto \lambda^2$ (equation 4), the stresses start to increase rapidly. So if fault-bounded blocks the size of those in Tibet were to rotate coherently, very substantial stresses would be necessary to maintain the topography. σ_{max} may also increase dramatically if T_e decreases. Although we assume T_e is approximately 15 km in Nevada (be-

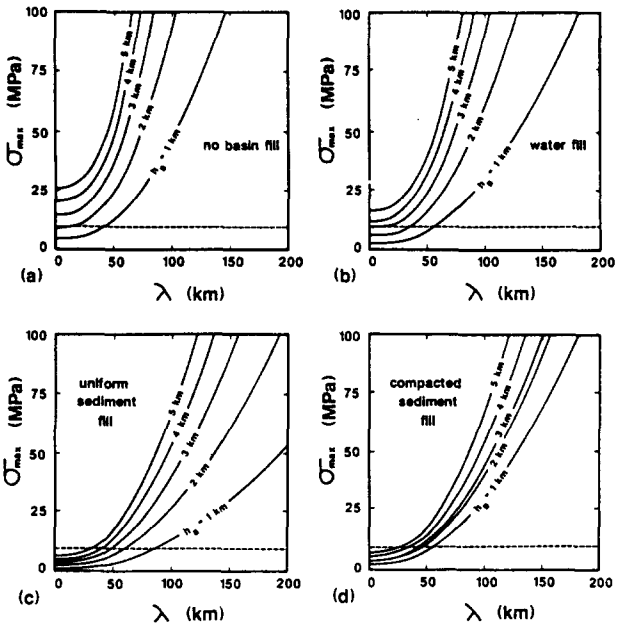

Fig. 10. The variation of σ_{max} as a function of λ, h_B and composition graben fill for a constant elastic thickness of 15 km. σ_{max} = 10 MPa, marked by the dashed line, is in the region of the maximum stress drop seen in earthquakes. (a) No basin fill; (b) water fill (density = 1.0 Mg m^{-3}); (c) uniform sediment fill (density = 2.0 Mg m^{-3}); (d) compacted sediment fill (grain density = 2.5 Mg m^{-3}, initial porosity, ϕ_0 = 60% and porosity decay length, l = 2 km.

cause earthquake foci occur to this depth: e.g. Doser 1986, Richens *et al.* 1987), it may in places be as small as 5 km (Bechtel & Forsyth 1987). If T_e = 5 km, then for $\lambda > 16$ km, $\sigma_{max} \propto \lambda^2$ and increases rapidly (Table 1).

In most of the examples given in Table 1 the sediment thickness in the graben (h_s) is poorly known, and several different values are given. This matters little as the greatest density contrast, and hence effect on σ_{max}, is produced by the surface topography (h_a). Thus the stresses in the Viking Graben are far smaller than they would otherwise be at their small dimensionless wavenumber (k') because all the crests are buried.

The values of σ_{max} in Table 1 and Fig. 10 are noteworthy. Blocks up to about 30 km in width may rotate coherently without requiring stresses greater than the stress drops observed to occur in earthquakes, which are typically in the range 1–10 MPa (10–100 bars: see e.g. Hanks 1977). Fault spacings substantially larger than this require much greater supporting stresses if the intervening blocks are to rotate coherently, and they probably do not do so, as stretched continental regions generally appear to have very little flexural strength (Barton & Wood, 1984). This simple analysis suggests that an upper limit to the size of rotating blocks in extending terranes is imposed by the thickness (or strength) of the outer elastic layer of the lithosphere. Fault-bounded blocks larger than the limiting size for a particular elastic thickness are expected to either break up, perhaps by antithetic faulting (possibly seen in

Table 1. Estimates of the maximum stress required to maintain a saw-tooth ('domino') topography, as a function of wavelength (λ), elastic thickness (T_e) and amplitude (see Fig. 9). Estimates of block widths, graben depth and fill are all approximate and taken from Jackson & McKenzie (1983), Gans *et al.* (1985), Armijo *et al.* (1986), Giltner (1988) and Jackson *et al.* (1988). Calculations in the Viking Graben assume the blocks are buried under 3 km of Tertiary sediment. We assume that: ρ_B = 2.85 Mg m^{-3}, ρ_s = 2.7 Mg m^{-3}, l = 2 km and ϕ_0 = 0.5

	T_e (km)	λ (km)	k'	h_a (m)	h_w (m)	h_s (m)	h_c (m)	h_B (m)	Δt (m)	σ_{max} (MPa)
Gulf of Suez (Gebel Zeit)	15	25	1.88	500	100	3500	2860	4000	1140	6.5
Nevada (Spring Valley)	15	30	1.57	1200	0	3000	2379	4200	1821	12.4
				1200	0	2500	1943	3700	1757	11.9
				2000	0	2500	1943	4500	2557	17.4
	5	30	0.52	1200	0	3000	2379	4200	1821	72.0
Central Greece	15	40	1.18	2000	100	4000	3646	6100	2454	22.2
				2000	600	4000	3821	6600	2779	25.1
				2000	600	2500	2154	5100	2946	26.7
				1000	600	2500	2154	4100	1946	17.6
Tibet	15	100	0.47	2000	0	2000	1515	4000	2485	120.2
				1000	0	2000	1515	3000	1485	71.8
				1000	0	3000	2379	4000	1621	78.4
	15	200	0.24	2000	0	2000	1515	4000	2485	461.1
Viking Graben (E. Shetland Terrace)	5	20	0.79	0	0	2000	1810	2000	190	3.3

Greece and parts of East Africa: see Jackson & McKenzie 1983, Rosendahl *et al.* 1986), or to form smaller 'dominoes', or simply to allow the footwall uplift and hangingwall subsidence to decay with distance from the fault at a rate dependent on the flexural strength, as described by Heiskanen & Vening Meinesz (1958). If block rotation occurs in places of high heat flow, such as at mid-ocean ridges, where both the seismogenic and elastic thickness are expected to be small, then λ might also be expected to be small to prevent k' from becoming too small (and hence σ_{max} too large). It may then be less surprising that in Afar the block spacing is as little as 1–2 km (Morton & Black 1975).

(b) *Continuity along strike.* We argued earlier that the available evidence suggests that large normal faults are rarely continuous along strike for more than about 20 km. It is natural to seek an explanation for this observation, and also obvious that this dimension, or maximum segment length, is comparable with the thickness of the upper seismogenic crust. Though it seems intuitively reasonable that the thickness of the deforming layer should influence the length and continuity of the structures that form within it, in the particular case of normal faults forming and continuing to move in the upper crust, we are unable to offer any theoretical support for this instinct. For the moment we simply point out the apparent similarity in size between the maximum fault segment length and the thickness of the upper seismogenic crust.

An important feature of active normal faulting is that it is distributed over wide regions. The slip vectors revealed in fault plane solutions are rarely pure dip-slip, and often show a small component of strike-slip (with slip vectors up to about 15° off the down-dip direction). Because the normal faulting is distributed, the strike-slip component is as well, thus distributing a simple shear (in plan view) across the deforming region. This, in turn, is likely to cause rotations about a vertical axis (e.g. Jackson & McKenzie 1983, 1984), which have been observed in some extensional terranes by paleomagnetic studies (e.g. Kissel *et al.* 1986, Hudson & Geissman 1987). Because the blocks also rotate about a horizontal axis, due to tilting, the overall rotation they experience is about an axis that is neither horizontal nor vertical, but inclined to the Earth's surface. Under these circumstances it is perhaps not surprising that the blocks (and faults) break up along strike, or, viewed another way, that there is a maximum size over which such rotations can be coherent; the size being limited by the strength of the outer elastic layer. If this suggestion is correct, it is perhaps reasonable that the maximum width of a block should be similar to its maximum length.

Estimating extension from faulting

It is now 10 years since McKenzie (1978a) proposed that lithospheric stretching played an important part in the formation of some continental sedimentary basins, and the controversy about whether that extension could be reliably estimated from observations of normal faulting dates from around that time. Since then our knowledge of normal fault geometry and evolution has increased considerably, particularly where active seismogenic normal faulting is concerned. Among the most important observations that now influence the debate are: (i) that earthquakes are confined to the upper crust; (ii) that large earthquakes do *not* occur on listric faults that flatten at shallow depths (as originally thought: e.g. McKenzie 1978a,b), but on faults that are steep throughout the seismogenic upper crust; (iii) that basement faults may be decoupled from those in the sedimentary cover; and (iv) that more than one generation of normal faults may have been active. Using present-day normal faulting as a guide, our approach to the problem of estimating regional extension from upper crustal faulting in terrains that are no longer active would begin by asking a series of questions.

(1) Is the size of the structure or region of interest comparable with (or larger than) the thickness of the seismogenic upper crust?

(2) At what level within the crust are the structures we are concerned with? Where was the seismic–aseismic transition *at the time the structures were active?*

(3) Are (or were) the structures of interest in the basement or sedimentary cover?

(4) Are there any weak layers controlled by lithology (e.g. overpressured shale or salt) that may decouple structures above from those below?

(5) What was the orientation of the structure *at the time it was active?*

The answers to these questions would determine the subsequent strategy, which broadly speaking, depends on whether the extension is to be estimated from large basement faults or faults restricted to the sedimentary cover.

(a) *Large basement faults.* The most surprising observation from regions of present-day extension is that the dips of large seismogenic normal faults are restricted to the same range (roughly 30–60°) everywhere on the continents. This appears to be true regardless of the reasons for the extension: the forces responsible for the extension in the Aegean Sea, which is underwater and next to a subduction zone, are different from those in Tibet, which is 5 km above sea level and next to a continental indenter (India), yet in both cases the seismogenic normal faulting is confined to the above dip range. The geometry of the faulting in the upper crust appears to be independent of the dynamics, and so the present-day pattern of faulting should be a useful guide to that in the past. For this reason, we believe that in regions of distributed faulting and tilting, where fault spacings are up to about 30 km, the simple rotating domino model is a most useful guide to the average extension, which can then be estimated from the fault dips and associated tilting, using equation (1). Applying this model is always likely to underestimate the true extension as it assumes the faults are planar, whereas they may well have a small amount of curvature, which increases the extension (Fig. 6). The observed range of

seismogenic fault dips cannot account for extension much greater than $\beta = 2$, and so in places where it is thought extension might exceed this value, the possibility of more than one generation of normal faults should be examined closely. Most regions of very high extension are underwater, particularly on continental margins, and it is improbable that the highly tilted blocks bounded by first generation faults will be imaged by seismic reflection techniques, though the later faults, which offset gently dipping sediments, may well be clear. Ignoring earlier generations of faulting will greatly underestimate the overall extension.

(b) *Faults in the sedimentary cover.* Such faults often flatten onto a weak layer at depth, and their shape in cross-section usually requires the surrounding blocks, particularly the hangingwall, to deform internally. Unless this internal deformation can be assessed it is not possible to determine accurately the overall extension. In general, this problem is indeterminate, as there is usually one observation (a bed in cross-section) and two unknowns (the shape of the fault and the inclination of simple shear in the hangingwall), and solutions are highly non-unique. If more than one bed shape is observed it may be possible to narrow the range of acceptable solutions considerably (White 1987, 1988). Ignoring the internal deformation of the hangingwall, or assuming vertical simple shear within it, may lead to a dramatic underestimate in the overall extension (perhaps as much as a factor of 2).

In short, estimating regional extension from normal faulting in the upper crust is not straightforward. Most importantly, because of the difficulty of accounting for extension that is not confined to slip on the major faults, whether in basement or sedimentary cover, most estimates will be too low. Underestimates by up to a factor of 2 are likely to be quite common.

CONCLUSIONS

We have attempted to summarize what is known about active normal faulting on the continents. The most important observation is that clear geometrical patterns are seen that are independent of the driving forces responsible for the extension, which vary considerably in their origin and magnitude. For this reason, patterns of active normal faulting today should provide a useful guide for the interpretation of normal faulting in older, now inactive terrains.

Earthquakes are largely confined to the upper 10–20 km of crust in regions of active extension. The thickness of the seismogenic upper layer, whose base is defined by the cutoff of microearthquakes, imposes a length scale on the faulting. Large normal faulting earthquakes move faults whose lengths are comparable to or bigger than the thickness of the seismogenic layer. These faults are approximately planar in cross-section, cut the base of the seismogenic layer and rotate about a horizontal axis as they move. The great majority have dips in the range 30–60°, and dips significantly less than 20° have not been observed. They are rarely continuous along strike for more than 15–20 km, but commonly curve or step in an en échelon fashion. Such changes along strike affect the lateral extent of rupture in earthquakes, allowing long fault systems to develop as a set of segmented shorter faults. The segmentation is an important influence on sedimentation and drainage. A reasonable estimate of regional extension can often be made from the dip of the larger faults and the tilt of the blocks they bound (the 'domino model'), but faults restricted to the dip range 30–60° cannot account for extension significantly greater than $\beta = 2$. Where extension exceeds this value, something else must happen: one possibility is that a second generation of steep faults starts to move. Small earthquakes, which move faults small compared with the seismogenic layer thickness, show no simple pattern and often indicate internal deformation of the blocks bounded by large faults.

Large seismogenic basement faults do not always reach the Earth's surface because they may be decoupled from the sedimentary cover by lithologically weak layers. Faults confined to the sedimentary cover do not appear to generate large earthquakes and can be strongly curved (listric) in cross-section. Estimating regional extension from such faulting requires a knowledge of the internal deformation of the hangingwall blocks, and is rarely straightforward or well constrained.

The most important influence on basement normal faulting in extensional terrains is probably the thickness and strength of the seismogenic upper layer, which, we believe, limits the maximum size of blocks ('dominoes') that rotate coherently about a horizontal axis and also limits the maximum continuity (segment length) of normal faults along strike.

Acknowledgements—The ideas in this paper owe much to discussions with R. B. Smith, R. Bruhn, D. McKenzie, S. Roberts, M. Leeder, P. Gans, E. Miller and J. Nabalek, to whom we are grateful. Dan McKenzie suggested the use of equation (4). H. Anderson, N. Kusznir, H. Lyon-Caen, J. Nabalak, C. Scholz and R. Westaway generously supplied preprints of their work. This work was supported by the Natural Environment Research Council, by NSF Contract EAR 8400470 (to R. B. Smith for support of J. A. Jackson at the Department of Geology & Geophysics, University of Utah) and by Sun Oil (Britain). N. J. White was supported by a British Council Studentship, by Merlin Geophysical Ltd, and by BIRPS. Department of Earth Sciences Contribution No. 1268.

REFERENCES

Aki, K. 1979. Characteristics of barriers on earthquake faults. *J. geophys. Res.* **84**, 6140–6148.

Aki, K. & Richards, P. G. 1980. *Quantitative Seismology*. Freeman, San Francisco.

Allen, C. R., Gillespie, A. R., Han Yuan, Sieh, K. E., Zhang Buchun & Zhu Chengnan. 1984. Red River and associated faults, Yunnan province, China: Quaternary geology, slip rates and seismic hazard. *Bull. geol. Soc. Am.* **95**, 686–700.

Ambraseys, N. N. & Tchalenko, J. 1972. Seismotectonic aspects of the Gediz, Turkey, earthquake of March 1970. *Geophys. J. R. astr. Soc.* **30**, 229–252.

Anderson, E. M. 1951. *The Dynamics of Faulting* (2nd Edn). Oliver & Boyd, Edinburgh.

Anderson, H. J. & Jackson, J. A. 1987. Active tectonics of the Adriatic region. *Geophys. J. R. astr. Soc.* **91**, 937–983.

Anderson, H. J. & Webb, T. In press. The rupture process of the

Edgecumbe earthquake, March 2, 1987, New Zealand. *Proc. R. Soc. N. Z.*

Armijo, R., Tapponnier, P., Mercier, J. & Han Tong-Lin. 1986. Quaternary extension in southern Tibet: field observations and tectonic implications. *J. geophys. Res.* **91**, 13,803–13,872.

Bache, T. C., Lambert, D. G. & Barker, T. G. 1980. A source model for the March 28, 1975, Pocatello valley earthquake from time-domain modelling of teleseismic P waves. *Bull. seism. Soc. Am.* **70**, 405–418.

Barr, D. 1987a. Lithosphere stretching, detached normal faulting and footwall uplift. In: *Continental Extensional Tectonics* (edited by Coward, M. P., Dewey, J. F. & Hancock, P. L.). *Spec. Publs geol. Soc. Lond.* **28**, 75–94.

Barr, D. 1978b. Structure/stratigraphic models for extension basins of half graben type. *J. Struct. Geol.* **9**, 491–500.

Barrientos, S. E., Stein, R. S. & Ward, S. N. 1987. Comparison of the 1959 Hebgen Lake, Montana and the 1983 Borah Peak, Idaho, earthquakes from geodetic observations. *Bull. seism. Soc. Am.* **77**, 784–808.

Barton, P. & Wood, R. 1984. Tectonic evolution of the North Sea basin: crustal stretching and subsidence. *Geophys. J. R. astr. Soc.* **79**, 987–1022.

Bechtel, T. D. & Forsyth, D. W. 1987. Isostatic compensation in the Basin and Range, U.S.A. (abstract). *EOS, Trans. Am. Geophys. Un.* **68**, 1450.

Bechtel, T. D., Forsyth, D. W. & Swain, C. J. 1987. Mechanisms of isostatic compensation in the vicinity of the East African Rift, Kenya. *Geophys. J. R. astr. Soc.* **90**, 445–465.

Bruhn, R. L., Gibler, P. R. & Parry, W. T. 1987. Rupture characteristics of normal faults: an example from the Wasatch fault zone, Utah. In: *Continental Extensional Tectonics* (edited by Coward, M. P., Dewey, J. F. & Hancock, P. L.). *Spec. Publs geol. Soc. Lond.* **28**, 337–353.

Butler, R., Stewart, G. S. & Kanamori, H. 1979. The July 27, 1976 Tangshan, China earthquake—a complex sequence of intraplate events. *Bull. seism. Soc. Am.* **69**, 207–220.

Chamberlain, R. M. 1983. Cenozoic domino-style crustal extension in the Lemitar mountains, New Mexico: a summary. In: *Socorro Region II* (edited by Chaplin, C. E.). *New Mexico geol. Soc. guidebook, 34th field conference,* 111–118.

Chen, W.-P., Nabalek, J. L., Fitch, T. J. & Molnar, P. 1981. An intermediate depth earthquake beneath Tibet: source characteristics of the event of September 14, 1976. *J. geophys. Res.* **86**, 2863–2876.

Chen, W.-P. & Molnar, P. 1983. Focal depths of intracontinental and intraplate earthquakes and their implications for the thermal and mechanical properties of the lithosphere. *J. geophys. Res.* **88**, 4183–4214.

Choy, G. L. & Kind, R. 1987. Rupture complexity of a moderate sized (m_b 6.0) earthquake: broadband body-wave analysis of the North Yemen earthquake of 13 December 1982. *Bull. seism. Soc. Am.* **77**, 28–46.

Crone, A. J. & Machette, M. N. 1984. Surface faulting accompanying the Borah Peak earthquake, central Idaho. *Geology* **12**, 664–667.

Das, S. 1982. Appropriate boundary conditions for modelling very long earthquakes and physical consequences. *Bull. seism. Soc. Am.* **72**, 1911–1926.

Davison, I. 1986. Listric normal fault profiles: calculation using bed-length balance and fault displacement. *J. Struct. Geol.* **8**, 209–210.

de Charpal, O., Guennoc, P., Montadert, L. & Roberts, D. G. 1978. Rifting, crustal attenuation and subsidence in the Bay of Biscay. *Nature* **275**, 706–711.

Deschamps, A. & King, G. C. P. 1983. The Campania–Lucania (southern Italy) earthquake of 23 November 1980. *Earth Planet Sci. Lett.* **62**, 296–304.

Deschamps, A. & King, G. C. P. 1984. Aftershocks of the Campania–Lucania (Italy) earthquake of 23 November 1980. *Bull. seism. Soc. Am.* **74**, 2483–2517.

Deschamps, A., Innaccone, G. & Scarpa, R. 1984. The Umbrian earthquake (Italy) of 19 September 1979. *Ann. Geophys.* **2**, 29–36.

Dorbath, C., Dorbath, L., Gaulon, R., George, T., Mourgue, P., Ramdani, M., Robineau, B. & Tadili, B. 1984. Seismotectonics of the Guinean earthquake of December 22, 1983. *Geophys. Res. Lett.* **11**, 971–974.

Doser, D. 1985. Source parameters and faulting processes of the 1959 Hebgen lake, Montana, earthquake sequence. *J. geophys. Res.* **90**, 4537–4555.

Doser, D. 1986. Earthquake processes in the Rainbow Mountain–Fairview Peak–Dixie valley, Nevada, region 1954–1959. *J. geophys. Res.* **91**, 12,572–12,586.

Doser, D. I. & Smith, R. B. 1985. Source parameters of the 28 October Borah Peak, Idaho, earthquake from body wave analysis. *Bull. seism. Soc. Am.* **75**, 1041–1051.

DSIR (Staff, New Zealand Department of Scientific and Industrial research) 1987. The March 2, 1987, earthquake near Edgecumbe, North Island, New Zealand. *EOS, Trans. Am. Geophys. Un.* **68**, 1161–1171.

Dziewonski, A. M. & Woodhouse, J. H. 1983. An experiment in systematic study of global seismicity: centroid moment tensor solutions for 201 moderate and large earthquakes in 1981. *J. geophys. Res.* **88**, 3247–3271.

England, P. C. & Jackson, J. A. 1987. Migration of the seismic–aseismic transition during uniform and non-uniform extension of the continental lithosphere. *Geology* **15**, 291–294.

Eyidoğan, H. 1983. Bitlis-Zağros bindirme ve kivrimli kuşağinin sismotektonik özellikleri. Unpublished Ph. D. thesis, Istanbul Technical University.

Eyidoğan, H. & Jackson, J. A. 1985. A seismological study of normal faulting in the Demirci, Alaşehir and Gediz earthquakes of 1969–1970 in western Turkey: implications for the nature and geometry of deformation in the continental crust. *Geophys. J. R. astr. Soc.* **81**, 569–607.

Fitch, T. J. & Muirhead, K. J. 1974. Depths to larger earthquakes associated with crustal loading. *Geophys. J. R. astr. Soc.* **37**, 285–296.

Fletcher, R. C. & Hallett, B. 1983. Unstable extension of the lithosphere: a mechanical model for Basin-and-Range structure. *J. geophys. Res.* **88**, 7457–7466.

Fraser, G. D., Witkind, I. J. & Nelson, W. H. 1964. A geological interpretation of the epicentral area–the dual basin concept. In: *The Hebgen Lake, Montana Earthquake of August* 17, 1959. *Prof. Pap. U.S. geol. Surv.* **435**, 99–106.

Gans, P. B. 1987. An open-system, two-layer crustal stretching model for the eastern Great Basin. *Tectonics* **6**, 1–12.

Gans, P. B. & Miller, E. L. 1983. Style of mid-Tertiary extension in east-central Nevada. *Utah Geol. & Min. Surv. Spec. Studies* **59**, 107–159.

Gans, P. B., Miller, E. L., McCarthy, J. & Ouldcott, M. L. 1985. Tertiary extensional faulting and evolving ductile-brittle transition zones in the northern Snake Range and vicinity: new insights from seismic data. *Geology* **13**, 189–193.

Garfunkel, Z. & Bartov, Y. 1977. The tectonics of the Suez rift. *Bull. geol. Surv. Israel* **71**.

Gasparini, C., Innacone, G., Scandone, P. & Scarpa, R. 1982. Seismotectonics of the Calabrian arc. *Tectonophysics* **84**, 267–286.

Gibbs, A. D. 1983. Balanced cross section construction from seismic sections in areas of extensional tectonics. *J. Struct. Geol.* **5**, 153–160.

Gibbs, A. D. 1984. Structural evolution of extensional basin margins. *J. geol. Soc. Lond.* **141**, 609–620.

Giltner, J. P. 1987. Application of extensional models to the North Viking Graben. *Norsk geol. Tidsskr.* **67**, 339–352.

Goff, J. A., Bergman, E. A. & Solomon, S. C. 1987. Earthquake source mechanisms and transform fault tectonics in the Gulf of California. *J. geophys. Res.* **92**, 10,485–10,510.

Grimison, N. L. & Chen, W.-P. 1988. Earthquakes in the Davie Ridge–Madagascar region and the southern termination of the Nubian–Somalian plate boundary. *J. geophys. Res.* **93**, 10, 439–10, 450.

Hanks, T. C. 1977. Earthquake stress drops, ambient tectonic stress, and stresses that drive plate motions. *Pure & Appl. Geophys.* **115**, 441–458.

Heiskanen, W. A. & Vening Meinesz, F. A. 1958. *The Earth and its Gravity Field.* McGraw-Hill, New York.

Hobbs, B. E., Ord, A. & Teyssier, C. 1986. Earthquakes in the ductile regime? *Pure & Appl. Geophys.* **124**, 309–336.

Huang, P. Y. & Solomon, S. C. 1987. Centroid depths and mechanisms of mid-ocean ridge earthquakes in the Indian Ocean, Gulf of Aden, and Red Sea. *J. geophys. Res.* **92**, 13161–1382.

Hudson, M. R. & Geissman, J. W. 1987. Paleomagnetic and structural evidence for middle Tertiary counterclockwise block rotation in the Dixie Valley region, west-central Nevada. *Geology* **15**, 638–642.

Huilan, Z., Liu, H.-L. & Kanamori, H. 1983. Source processes of large earthquakes along the Xianshuihe fault in southwestern China. *Bull. seism. Soc. Am.* **73**, 537–551.

Jackson, J. A. 1987. Active normal faulting and crustal extension. In: *Continental Extensional Tectonics* (edited by Coward, M. P., Dewey, J. F. & Hancock, P. L.). *Spec. Publs geol. Soc. Lond.* **28**, 3–17.

Jackson, J. A. & Fitch, T. J. 1981. Basement faulting and the focal

depths of the larger earthquakes in the Zagros mountains (Iran). *Geophys. J. R. astr. Soc.* **64**, 561–586.

Jackson, J. A., Gagnepain, J., Houseman, G., King, G., Papadimitriou, P., Soufleris, C. & Virieux, J. 1982a. Seismicity, normal faulting and the geomorphological development of the Gulf of Corinth (Greece): the Corinth earthquakes of February and March 1981. *Earth Planet Sci. Lett.* **57**, 377–397.

Jackson, J. A., King, G. & Vita-Finzi, C. 1982b. The neotectonics of the Aegean: an alternative view. *Earth Planet Sci. Lett.* **61**, 303–318.

Jackson, J. A. & McKenzie, D. P. 1983. The geometrical evolution of normal fault systems. *J. Struct. Geol.* **5**, 471–482.

Jackson, J. A. & McKenzie, D. P. 1984. Active tectonics of the Alpine–Himalayan belt between western Turkey and Pakistan. *Geophys. J. R. astr. Soc.* **77**, 185–264.

Jackson, J. A., White, N. J., Garfunkel, Z. & Anderson, H. 1988. Relations between normal-fault geometry, tilting and vertical motions in extensional terrains: an example from the southern Gulf of Suez. *J. Struct. Geol.* **10**, 155–170.

Jankhof, K. 1945. Changes in ground level produced by the earthquakes of April 14 and 18 1928 in southern Bulgaria. In: *Tremblements de Terre en Bulgarie*, Nos 29–31. Institut Meteorologique central de Bulgarie, Sofia, 131–136 (in Bulgarian).

Jemsek, J. P., Bergman, E. A., Nabalek, J. L. & Solomon, S. C. 1986. Focal depths and mechanisms of large earthquakes on the Arctic mid-ocean ridge system. *J. geophys. Res.* **91**, 13,993–14,005.

Kim, W.-Y., Kulhanek, O. & Meyer, K. 1984. Source processes of the 1981 Gulf of Corinth earthquake sequence from body-wave analysis. *Bull. seism. Soc. Am.* **74**, 459–477.

King, G. & Nabalek, J. 1985. Role of fault bends in the initiation and termination of earthquake rupture. *Science* **228**, 984–987.

Kissel, C., Laj, C. & Mazaud, A. 1986. First paleomagnetic results from Neogene formations in Evia, Skyros and the Volos regions, and the deformation in central Aegea. *Geophys. Res. Lett.* **13**, 1446–1449.

Kusznir, N. J. & Matthews, D. H. 1988. Deep seismic reflections and the deformational mechanisms of the continental lithosphere. *J. Petrol. Special Lithosphere Issue*, 63–87.

Langston, C. A. & Butler, R. 1976. Focal mechanism of the August 1, 1975 Oroville earthquake. *Bull. seism. Soc. Am.* **66**, 1111–1120.

Leeder, M. R. & Gawthorpe, R. L. 1987. Sedimentary models for extensional tilt-block/half-graben basins. In: *Continental Extensional Tectonics* (edited by Coward, M. P., Dewey, J. F. & Hancock, P. L.). *Spec. Publs geol. Soc. Lond.* **28**, 139–152.

Le Pichon, X. & Sibuet, J. C. 1981. Passive margins: a model of formation. *J. geophys. Res.* **86**, 3708–3721.

Lindh, G. & Boore, D. M. 1981. Control of rupture by fault geometry during the 1966 Parkfield earthquake. *Bull. seism. Soc. Am.* **71**, 95–116.

Lyon-Caen, H., Armijo, R., Drakopoulos, J., Baskoutass, J., Delibassis, N., Gaulon, R., Kouskouna, V., Latoussakis, J., Makropoulos, K., Papadimitriou, P., Papanastassiou, D. & Pedotti, G. In press. The 1986 Kalamata (south Peloponnesus) earthquake: detailed study of a normal fault and tectonic implications. *J. geophys. Res.*

Machette, M. N., Personius, S. F. & Nelson, A. R. 1986. Late Quaternary segmentation and slip rate history of the Wasatch Fault Zone, Utah (abstract). *EOS, Trans. Am. Geophys. Un.* **67**, 1107.

McKenzie, D. P. 1967. Some remarks on heat flow and gravity anomalies. *J. geophys. Res.* **72**, 6261–6273.

McKenzie, D. P. 1972. Active tectonics of the Mediterranean region. *Geophys. J. R. astr. Soc.* **30**, 109–185.

McKenzie, D. P. 1978a. Some remarks on the development of sedimentary basins. *Earth Planet Sci. Lett.* **40**, 25–32.

McKenzie, D. P. 1978b. Active tectonics of the Alpine–Himalayan belt: the Aegean Sea and surrounding regions. *Geophys. J. R. astr. Soc.* **55**, 217–254.

McKenzie, D. P. & Bickle, M. J. 1988. The volume and composition of melt generated by extension of the lithosphere. *J. Petrol.* **29**, 625–679.

McKenzie, D. P., Molnar, P. & Davies, D. 1970. Plate tectonics of the Red Sea and East Africa. *Nature* **226**, 243–248.

McNutt, M. 1980. Implications of regional gravity for state of stress in the Earth's crust and upper mantle. *J. geophys. Res.* **85**, 6377–6396.

Meissner, R. & Strehlau, J. 1982. Limits of stress in continental crust and their relation to the depth–frequency relation of shallow earthquakes. *Tectonics* **1**, 73–89.

Molnar, P. & Chen, W.-P. 1983. Focal depths and fault plane solutions of earthquakes under the Tibetan plateau. *J. geophys. Res.* **88**, 1180–1196.

Molnar, P. & Deng, Q. 1984. Faulting associated with large earthquakes and the average rate of deformation in central and eastern Asia. *J. geophys. Res.* **89**, 6203–6227.

Moore, J. G. 1960. Curvature of normal faults in the Basin and Range Province of the western United States. *Prof. Pap. U.S. geol. Surv.* **400**, 409–411.

Morton, W. H. & Black, R. 1975. Crustal attenuation in Afar. In: *Afar Depression of Ethiopia* (edited by Pilger, A. & Rosler, A.). *Inter-Union comm. Geodyn. Sci. Rep.* **14**, 55–65. Schweizerbart'sche Verlagsbuchhandlung, Stuttgart.

Myers, W. B. & Hamilton, W. 1964. Deformation accompanying the Hebgen Lake earthquake of August 17, 1959. *Prof. Pap. U.S. geol. Surv.* **435**, 55–98.

Nabalek, J. In press. Planar vs listric faulting: the rupture process and fault geometry of the 1983 Borah Peak, Idaho earthquake from inversion of teleseismic body waves. *J. geophys. Res.*

Nabalek, J., Chen, W.-P. & Hong, Ye. 1987. The Tangshan earthquake sequence and its implications for the evolution of the North China Basin. *J. geophys. Res.* **92**, 12,615–12,628.

Nelson, M. R., McCaffrey, R. & Mohnar, P. 1987. Source parameters for 11 earthquakes in the Tien Shan, central Asia, determined by P and SH waveform inversion. *J. geophys. Res.* **92**, 12,629–12,648.

North, R. 1977. Seismic moment, source dimension and stresses associated with earthquakes in the Mediterranean and Middle East. *Geophys. J. R. astr. Soc.* **48**, 137–161.

Proffett, J. M. 1977. Cenozoic geology of the Yerington district, Nevada, and implications for the Nature of Basin and Range faulting. *Bull. geol. Soc. Am.* **88**, 247–266.

Ransome, F. L., Emmons, W. H. & Garrey, G. H. 1910. Geology and ore deposits of the Bullfrog district, Nevada. *Bull. U.S. geol. Surv.* **407**, 1–130.

Richens, W. D., Pechmann, J. C., Smith, R. B., Langer, C. J., Goter, S. K., Zollweg, J. E. & King, J. J. 1987. The 1983 Borah Peak, Idaho, earthquake and its aftershocks. *Bull. seism. Soc. Am.* **77**, 694–723.

Richter, C. F. 1958. *Elementary Seismology*. W. H. Freeman, San Francisco.

Romney, C. 1957. Seismic waves from the Dixie Valley–Fairview Peak earthquakes. *Bull. seism. Soc. Am.* **47**, 301–319.

Rosendahl, B. R., Reynolds, D. J., Lorber, P. M., Burgess, C. F., McGill, J., Scott, D., Lambiase, J. J. & Derksen, S. J. 1986. Structural expressions of rifting: lessons from Lake Tanganyika, Africa. In: *Sedimentation in the African Rifts* (edited by Frostick, L. E., Renaut, R. W., Reid, I. & Tiercelin, J. J.). *Spec. Publs geol. Soc. Lond.* **25**, 29–43.

Rutter, E. H. 1986. On the nomenclature of mode of failure transitions in rocks. *Tectonophysics* **122**, 381–387.

Savage, J. C. & Hastie, L. M. 1966. Surface deformation associated with dip slip faulting. *J. geophys. Res.* **71**, 4897–4904.

Scholz, C. H. 1982. Scaling laws for large earthquakes: consequences for physical models. *Bull. seism. Soc. Am.* **72**, 1–14.

Scholz, C. H. 1988. The brittle–plastic transition and the depth of seismic faulting. *Geol. Rdsch.* **77**, 319–328.

Schwarz, D. P. & Coppersmith, K. J. 1984. Fault behaviour and characteristic earthquakes: examples from the Wasatch and San Andreas fault zones. *J. geophys. Res.* **89**, 5681–5698.

Sclater, J. G. & Christie, P. A. F. 1980. Continental stretching: an explanation of the post mid-Cretaceous subsidence of the Central North Sea basin. *J. geophys. Res.* **85**, 3711–3739.

Seeber, L. & Armbruster, J. 1981. Great detachment earthquakes along the Himalayan arc and long term forecasts. In: *Earthquake Prediction* (edited by Simpson, D. W. & Richards, P. G.). *Am. Geophys. Un.*, 259–277.

Shimazaki, K. 1986. Small and large earthquakes: the effects of the thickness of the seismogenic layer and the free surface. In: *Earthquake Source Mechanics* (edited by Das, S., Boatwright, J. & Scholz, C. H.). *Am. Geophys. Un.*, 209–216.

Shirokova, E. I. 1972. Stress pattern and probable motion in the earthquake foci of the Asia–Mediterranean seismic belt. In: *Elastic Strain Field of the Earth and Mechanisms of Earthquake Sources.* Seismology No. 8 (edited by Balakina, L. M. *et al.*). Nauka Press, Moscow.

Shudofsky, G. N. 1985. Source mechanisms and focal depths of east African earthquakes using Rayleigh wave inversion and body wave modelling. *Geophys. J. R. astr. Soc.* **83**, 563–614.

Sibson, R. H. 1980. Transient discontinuities in ductile shear zones. *J. Struct. Geol.* **2**, 165–171.

Sibson, R. H. 1982. Fault zone models, heat flow, and the depth distribution of earthquakes in the continental crust of the United States. *Bull. seism. Soc. Am.* **72**, 151–163.

Sibson, R. H. 1985. A note on fault reactivation. *J. Struct. Geol.* **7**, 751–754.

Slemmons, D. B. 1957. Geological effects of the Dixie Valley–Fairview Peak, Nevada, earthquakes of December 16, 1954. *Bull. seism. Soc. Am.* **47**, 353–375.

Smith, R. B. & Sbar, M. L. 1974. Contemporary tectonics and seismicity of the western United States with emphasis on the Intermountain seismic belt. *Bull. geol. Soc. Am.* **85**, 1205–1218.

Soufleris, C. & Stewart, G. S. 1981. A source study of the Thessaloniki (northern Greece), 1978 earthquake sequence. *Geophys. J. R. astr. Soc.* **67**, 343–358.

Spencer, J. E. & Reynolds, S. J. In press. Middle Tertiary tectonics of Arizona and the south-west. *Arizona geol. Soc. dig.* **17**.

Stein, R. S. & Barrientos, S. E. 1985. Planar high angle faulting in the Basin & Range: geodetic analysis of the 1980 Borah Peak, Idaho earthquake. *J. geophys. Res.* **90**, 11,355–11,366.

Stewart, J. H. 1980. Regional tilt patterns of the late Cenozoic basin-range fault blocks, western United States. *Bull. geol. Soc. Am.* **91**, 46–464.

Stewart, G. S. & Kanamori, H. 1982. Complexity of rupture in large strike-slip earthquakes in Turkey. *Phys. Earth & Planet. Interiors* **28**, 70–84.

Stoker, S. J. & Brown, S. 1986. Lithofacies of late Jurassic coarse clastic sediments of the south Viking Graben, northern North Sea: a core workshop. *Mar. Earth Sci. Directorate, Open File Report, British Geol. Surv.*

Strehlau, J. 1986. A discussion of the depth extent of rupture in large continental earthquakes. In: *Earthquake Source Mechanics* (edited by Das, S., Boatwright, J. & Scholz, C. H.). *Am. Geophys. Un.*, 131–145.

Swan, F. H. III, Schwarz, D. P. & Cluff, L. S. 1980. Recurrence of moderate-to-large magnitude earthquakes produced by surface faulting on the Wasatch Fault zone. *Bull. seism. Soc. Am.* **70**, 1431–1462.

Tapponnier, P. & Molnar, P. 1977. Active faulting and Cenozoic tectonics of China. *J. geophys. Res.* **82**, 2905–2930.

Tapponnier, P. & Molnar, P. 1979. Active faulting and Cenozoic tectonics of the Tien Shan, Mongolia, and Baykal regions. *J. geophys. Res.* **84**, 3425–3459.

Tse, S. & Rice, J. 1986. Crustal earthquake instability in relation to the depth variation of frictional properties. *J. geophys. Res.* **91**, 9452–9472.

Verrall, P. 1981. *Structural Interpretation with Application to North Sea Problems.* Course notes No. 3, Joint Ass. for Petroleum Exploration courses (U.K.).

Vvedenskaya, A. V. & Balakina, L. M. 1960. Methods and results of the determination of stresses acting in the foci of earthquakes of Pribaykal and Mongolia (in Russian). *Bull Sov. Seismol. Acad. Sci. U.S.S.R.* **9**, 73–84.

Wagner, G. S. & Langston, C. A. 1986. Waveform inversion of five African earthquakes and tectonic implications for continental deformation (abstract). *EOS, Trans. Am. Geophys. Un.* **67**, 304.

Wallace, R. 1984. Fault scarps formed during the earthquakes of October 2 1915 in Pleasant Valley, Nevada, and some tectonic implications. *Prof. Pap. U.S. geol. Surv.* **1274A**, 1–33.

Watts, A. B. 1988. Gravity anomalies, crustal structure and flexure of the lithosphere at the Baltimore Canyon Trough. *Earth Planet. Sci. Lett.* **89**, 221–238.

Wernicke, B. 1981. Low angle normal faults in the Basin and range province: nappe tectonics in an extending orogen. *Nature* **291**, 645–648.

Wernicke, B. 1985. Uniform sense normal simple shear of the continental lithosphere. *Can. J. Earth Sci.* **22**, 108–125.

Wernicke, B. & Burchfiel, B. C. 1982. Modes of extensional tectonics. *J. Struct. Geol.* **4**, 105–115.

Westaway, R. 1987. The Campania, southern Italy, earthquakes of 1962 August 21. *Geophys. J. R. astr. Soc.* **88**, 1–24.

Westaway, R. & Jackson, J. A. 1987. The earthquake of 1980 November 23 in Campania–Basilicata (southern Italy). *Geophys. J. R. astr. Soc.* **90**, 375–443.

White, N. 1987. Constraints on the measurement of extension in the brittle upper crust. *Norsk. geol. Tidsskr.* **67**, 269–279.

White, N. J. 1988. Extension and subsidence of the continental lithosphere. Unpublished Ph.D. thesis, University of Cambridge.

White, N. J., Jackson, J. A. & McKenzie, D. P. 1986. The relationship between the geometry of normal faults and that of the sedimentary layers in their hanging walls. *J. Struct. geol.* **8**, 897–909.

White, R. S., Spence, G. D., Fowler, S. R., McKenzie, D. P., Westbrook, G. K. & Bowen, A. N. 1987. Magmatism at rifted continental margins. *Nature* **330**, 439–444.

Wiens, D. A. & Stein, S. 1983. Age dependence of oceanic intraplate seismicity and implications for lithospheric evolution. *J. geophys. Res.* **88**, 6455–6468.

Williams, G. & Vann, I. 1987. The geometry of listric normal faults and deformation in their hanging walls. *J. Struct. Geol.* **9**, 789–795.

Yielding, G. 1985. Control of rupture by fault geometry during the 1980 El Asnam (Algeria) earthquake. *Geophys. J. R. astr. Soc.* **81**, 641–670.

Ziegler, P. 1982. *Geological Atlas of Western and Central Europe.* Shell Int. Petrol. Maats. B.V., The Hague.

Ziegler, P. 1983. Crustal thinning and subsidence in the North Sea. *Nature* **304**, 561.

Zollweg, J. E. & Richens, W. D. 1985. Later aftershocks of the 1983 Borah Peak, Idaho, earthquake and related activity in central Idaho. In: *Proc. Workshop XXVIII on the Borah Peak, Idaho, Earthquake* (edited by Stein, R. S. & Bucknam, R. C.). *U.S. Geol. Surv., Open-file Rept* 85-290, 345–367.

APPENDIX

This Appendix contains the data upon which Fig. 1 is based.

Table A1. Epicentral information for each earthquake, identified by number and grouped by region. The numbered references to each earthquake (right-hand column) are identified in Table A3. If more than one reference is given, the first one is that used for the focal parameters in Table A2

No.	Date	Time	Lat.	Long.	Region	Ref.
101	1915.10.03	06:53	40.50	-117.50	W. USA, NV	1
102	1954.08.24	05:51	39.50	-118.30	W. USA, NV	2
103	1954.12.16a	11:11	39.80	-118.10	W. USA, NV	2,3
104	1954.12.16b	11:07	39.28	-118.13	W. USA, NV	2,3,4,5
105	1959.08.18	06:37	44.80	-111.10	W. USA, MO	6,7
106	1962.08.30	13:35	41.80	-111.80	W. USA, UT	8,9
107	1969.03.20	08:17	31.32	-114.18	Gulf of Calif.	10
108	1969.03.21	06:34	31.25	-114.31	Gulf of Calif.	10
109	1975.08.01	20:20	39.50	-121.47	W. USA, CA	11
110	1975.03.28	02:31	42.04	-112.41	W. USA, ID	12
111	1983.10.28a	14:06	43.98	-113.90	W. USA, ID	13,14,15
112	1983.10.28b	19:51	44.07	-113.89	W. USA, ID	16,32
113	1983.10.29	23:29	44.24	-114.07	W. USA, ID	16,32
114	1984.08.22	09:46	44.38	-114.08	W. USA, ID	17
115	1984.09.08	06:16	44.44	-114.15	W. USA, ID	32
116	1986.07.20	14:29	37.58	-118.45	W. USA, CA	32
117	1986.07.21a	14:42	37.54	-118.45	W. USA, CA	32
118	1986.07.21b	22:07	37.49	-118.40	W. USA, CA	32
201	1966.03.06	02:15	31.49	80.50	Tibet	18
202	1966.10.14	01:04	36.45	87.43	Tibet	18
203	1971.05.03	00:33	30.79	84.33	Tibet	18
204	1973.07.14a	04:51	35.18	86.48	Tibet	18
205	1973.07.14b	13:39	35.26	86.60	Tibet	18
206	1973.08.01	01:14	29.59	89.17	Tibet	18
207	1973.08.16	08:02	33.24	86.84	Tibet	18
208	1973.09.08	07:25	33.29	86.82	Tibet	18
209	1975.01.19	08:01	32.39	78.50	Tibet	18
210	1975.04.28	11:06	35.82	79.92	Tibet	18
211	1975.05.19	19:47	35.16	80.80	Tibet	18
212	1975.06.04	02:24	35.87	79.85	Tibet	18
213	1975.07.19	06:10	31.92	78.61	Tibet	18
214	1975.07.29	02:40	32.56	78.46	Tibet	18
215	1976.09.14	06:43	29.81	89.57	Tibet	19
301	1966.09.28	14:00	27.53	100.08	S.W. China	20
302	1967.08.30a	04:22	31.60	100.31	S.W. China	21
303	1967.08.30b	11:08	31.60	100.31	S.W. China	21
304	1973.02.07	16:06	31.46	100.29	S.W. China	21
305	1986.03.13	08:41	26.20	100.09	S.W. China	32
401	1957.06.27	00:09	56.31	116.99	Baykal, USSR	22,60
402	1958.01.05	11:30	56.50	121.23	Baykal, USSR	22
403	1958.09.14	14:21	56.67	121.01	Baykal, USSR	22
404	1967.01.18	05:34	56.68	120.95	Baykal, USSR	23
405	1971.06.14	13:48	56.18	123.59	Baykal, USSR	23
406	1987.02.21	22:19	54.93	110.98	Baykal, USSR	32
501	1976.07.28	10:45	39.71	118.37	N.E. China	24,25
502	1976.08.31	03:25	39.91	118.90	N.E. China	24
503	1977.03.07	00:28	40.10	118.74	N.E. China	24
504	1987.08.10	12:12	38.12	106.36	N.E. China	32
601	1962.08.21a	18:09	41.20	15.00	Italy	26
602	1962.08.21b	18:19	41.25	15.05	Italy	26
603	1979.09.19	21:35	42.81	13.06	Italy	27,28
604	1980.11.23	18:34	40.76	15.33	Italy	29,30,31
605	1984.04.29	05:03	43.26	12.56	Italy	32
606	1984.05.07	17:49	41.77	13.90	Italy	32
607	1984.05.11	10:41	41.83	13.96	Italy	32
711	1967.11.30	07:23	41.41	20.44	Aegean, Albania	27,35,36
712	1986.03.03	01:24	41.97	20.29	Aegean, Albania	32
721	1977.11.03	02:22	42.11	23.97	Aegean, Bulgaria	34
731	1963.07.26	04:17	42.10	21.40	Aegean, Yugoslavia	27,35,36
741	1954.04.30	13:02	39.24	22.17	Aegean, Greece	35
742	1956.07.09	03:11	36.69	25.81	Aegean, Greece	37
743	1965.04.27	14:09	35.70	23.50	Aegean, Greece	38,58
744	1965.07.06	03:18	38.40	22.40	Aegean, Greece	38,35
745	1965.12.20	00:08	40.20	24.80	Aegean, Greece	38,35
746	1966.02.05	02:01	39.02	21.82	Aegean, Greece	27,35,39
747	1967.03.04	17:58	39.20	24.60	Aegean, Greece	38,35
748	1967.05.01	07:09	39.70	21.30	Aegean, Greece	27,35
749	1968.12.05	07:52	36.58	26.97	Aegean, Greece	38,35
750	1970.04.08	13:50	38.43	22.66	Aegean, Greece	38,35
751	1975.04.04	05:16	38.09	21.98	Aegean, Greece	33
752	1978.05.23	23:34	40.76	23.27	Aegean, Greece	40
753	1978.06.19	10:31	40.75	23.22	Aegean, Greece	40
754	1978.06.20	20:03	40.74	23.23	Aegean, Greece	40
755	1979.06.14	11:44	38.81	26.53	Aegean, Greece	41
756	1980.07.10	19:39	39.31	22.93	Aegean, Greece	41
757	1981.02.24	20:53	38.10	22.84	Aegean, Greece	42,43
758	1981.02.25	02:35	38.14	23.05	Aegean, Greece	42,43
759	1981.03.04	21:58	38.14	23.05	Aegean, Greece	42,43
760	1984.02.11	08:02	38.40	22.09	Aegean, Greece	32
761	1984.07.09	18:57	40.68	21.83	Aegean, Greece	32
762	1985.04.30	18:14	39.26	22.81	Aegean, Greece	32
763	1985.11.09	23:30	41.26	23.99	Aegean, Greece	32
764	1986.09.13	17:24	37.01	22.18	Aegean, Greece	32,58
765	1987.02.23	23:34	38.47	20.29	Aegean, Greece	32
780	1955.07.16	07:07	37.66	27.19	Aegean, Turkey	35
781	1956.02.20	20:31	39.86	30.49	Aegean, Turkey	35
782	1963.09.18	16:48	40.90	29.20	Aegean, Turkey	44,35
783	1964.06.14	12:15	38.00	38.50	Aegean, Turkey	45
784	1964.10.06	14:31	40.30	28.20	Aegean, Turkey	35,46
785	1965.06.13	20:01	37.80	29.30	Aegean, Turkey	38,35
786	1967.07.30	01:31	40.70	30.40	Aegean, Turkey	38,35
787	1969.03.23	21:08	39.16	28.48	Aegean, Turkey	47,35
788	1969.03.25	13:21	39.18	28.37	Aegean, Turkey	47,35
789	1969.03.28	01:48	38.59	28.45	Aegean, Turkey	47,35,36
790	1969.04.06	03:49	38.50	26.42	Aegean, Turkey	38,35
791	1969.04.30	20:20	39.16	28.58	Aegean, Turkey	47,35
792	1970.03.28a	21:02	39.20	29.47	Aegean, Turkey	47,33,36
793	1970.03.28b	23:11	39.22	29.52	Aegean, Turkey	33
794	1970.04.16	10:42	39.03	30.00	Aegean, Turkey	47,33
795	1970.04.19	19:13	39.06	29.83	Aegean, Turkey	47,33
796	1970.04.23	09:01	39.09	28.59	Aegean, Turkey	47,33
797	1971.05.12	06:25	37.59	29.76	Aegean, Turkey	33
798	1971.05.25	05:43	39.03	29.74	Aegean, Turkey	47,33
799	1972.03.14	14:05	39.28	29.42	Aegean, Turkey	47,33
800	1975.03.27	05:15	40.42	26.14	Aegean, Turkey	33
801	1986.10.11	09:00	37.93	28.57	Aegean, Turkey	32
901	1966.03.20	01:42	0.81	29.90	E. Africa	48,49
902	1966.05.06	02:36	-15.72	34.59	E. Africa	48
903	1966.05.17	07:03	0.76	29.95	E. Africa	48
904	1968.05.15	07:51	-15.91	26.16	E. Africa	48,49
905	1968.12.02	02:33	-14.01	23.82	E. Africa	48,49
906	1976.07.01	11:24	-29.51	25.17	S. Africa	48
907	1976.09.19	14:59	-11.08	32.84	E. Africa	48
908	1977.07.06	08:48	- 6.26	29.59	E. Africa	48
909	1977.12.15	23:20	- 4.80	34.92	E. Africa	48
910	1983.12.27	00:39	-18.25	44.86	Madagascar	32
911	1984.08.25	20:37	- 8.75	32.45	E. Africa	32
912	1984.10.26	07:44	-16.47	28.67	E. Africa	32
913	1985.05.14a	13:24	-10.59	41.37	E. Africa	50
914	1985.05.14b	18:11	-10.49	41.43	E. Africa	50
915	1985.06.28	22:46	- 2.47	28.91	E. Africa	32
916	1985.08.20	05:46	5.52	36.14	E. Africa	32
917	1986.06.29	21:47	- 5.34	29.54	E. Africa	32
918	1986.08.18	15:07	-16.36	28.50	E. Africa	32
919	1986.10.06	18:53	-30.55	28.74	S. Africa	32
920	1987.10.25	16:46	5.40	36.75	E. Africa	32
1001	1969.04.07	20:26	76.55	130.86	Laptev Sea	51
1002	1983.06.10	02:13	75.53	122.75	Laptev Sea	51
1021	1969.03.31	07:15	27.67	33.99	Gulf of Suez	52,53,54
1022	1972.06.28	09:49	27.65	33.76	Gulf of Suez	52,53,44
1031	1970.07.30	00:52	37.82	55.88	N.E. Iran	44
1041	1987.03.02	01:42	-37.91	176.79	New Zealand	59,55
1051	1982.12.13	09:12	14.71	44.38	Yemen	56
1061	1982.09.29	05:50	14.49	-89.12	Guatemala	32
1071	1983.12.22	04:11	11.87	13.53	Guinea	57
1081	1983.11.18	01:15	39.78	39.46	E. Turkey	32
1091	1985.04.10	20:15	1.56	-77.01	Colombia, Andes	32

Table A2. Focal parameters for each earthquake. The columns include: event number (from Table A1); body wave magnitude (m_b), surface wave magnitude (M_s) and seismic moment (M_o) in units of 10^{18} Nm (where available); whether the fault and auxiliary planes in the fault plane solution can be distinguished (+ = yes), usually by surface faulting (*F*); the strike (s), dip (d) and rake (r) of the first and second nodal planes of the fault plane solution, using the convention of Aki & Richards (1980): the first plane is the fault plane wherever it can be distinguished from the auxiliary plane; focal depth in km (dep), estimated from body wave modelling (*P, SH*) or *pP* arrivals (final column). An *m* after the focal depth indicates that the earthquake was identified as a multiple event from its seismograms. Most of the fault plane solutions are based primarily on the polarity of long-period *P* arrivals, some being additionally constrained by *SH* waveforms (last column). An H after the event number indicates that the solution is from a Harvard Centroid Moment Tensor Inversion (reported by the United States Geological Society), and is not included in Fig. 1(b). An asterisk (*) after the event number indicates a poorly constrained solution that is not included in Fig. 1. It is included here to identify it for future improvement. An asterisk (*) after the dip indicates that the dip of this nodal plane could be steeper (see Fig. 1b)

No.	m_b	M_s	M_o	f_p	s_1	d_1	r_1	s_2	d_2	r_2	dep	
102		6.8	6.9	+*F*	355	50	-145	242	64	-045	12*m*	*P, SH*
104		7.1	50.0	+*F*	350	60	-160	250	74	-031	15*m*	*P, SH*
105 *		7.5	100.0	+*F*	102	60	-090	282	30	-090	10*m*	*P, SH*
106	5.7		0.3		025	50	-080	190	41	-101	12	*P, SH*
107	5.3	5.7	0.5		023	43	-087	199	47	-093	6	*P, SH*
108	5.6	5.4	0.3		035	43	-086	210	47	-093	3	*P, SH*
109	5.8	5.6	0.6	+*F*	180	65	-070	319	32	-110	6	*P, SH*
110	6.1	6.0	2.2	+	225	39	-053	001	60	-116	9	*P*
111	6.2	7.3	32.0	+*F*	149	50	-067	297	45	-109	7	*P, SH*
112	5.4	5.1	0.3		189	77	-033	287	58	-165		
113	5.4	5.0	0.2		093	45	-117	309	51	-065		
114	5.0	5.1			153	50	-046	277	57	-129		
115 H	5.0	4.4	0.1		154	20	-071	314	71	-097		
116 H	5.6	5.6	0.6		223	54	-035	335	63	-138		
117 H	6.0	6.2	2.6		149	60	-163	051	75	-031		
118 H	5.5	5.0	0.1		040	45	-050	171	57	-122		
201	6.0	6.5	3.4		000	45*	-090	180	45	-090	8*m*	*P*
202	5.3	5.7	0.2		025	66	-090	205	24*	-090	8	*P*
203	5.4	5.7	0.3		190	58	-090	010	32*	-090	8	*P*
204	6.0	6.9	9.0		190	60	-145	081	60	-035	6*m*	*P*
205	5.9	5.5	4.0		037	68	-056	156	40	-144	7	*P*
206 *	4.9	4.5			220	60	-024	323	69	-148	85	*pP*
207	5.3	5.5	0.2		160	55	-155	055	70	-038	8	*P*
208	5.5	5.2	0.6		118	60	-171	018	74	-031	9	*P*
209	6.2	6.8	16.1		000	50	-090	180	40*	-090	9*m*	*P*
210	5.8	6.3	1.0		169	62	-149	063	63	-032	7	*P*
211	5.5	5.1	0.3		248	66	-050	004	46	-145	8	*P*
212	5.7	5.8	1.1		180	62	-121	052	41	-046	9	*P*
213	5.3	4.7	0.1		180	50	-125	047	51	-056	6	*P*
214	5.5	5.1	0.1		210	55	-090	030	35*	-090	8	*P*
215 *	5.5		0.9		215	52	-068	002	43	-116	90	*P*
301	6.1	6.2			290	45	-114	142	40	-068		
302	6.1	6.1	4.5		245	45	-070	038	48	-110	8	*P*
303	5.1	5.1	0.2		233	50	-090	053	40	-090	10	*P*
304	5.8	5.9	0.6		210	60	-090	030	30	-090	10	*P*
305 H	5.4	4.6	0.1		330	25	-104	165	66	-084		
401		7.9	100.0	+*F*	120	62	-034	228	62	-147		
402					295	62	-056	060	42	-136		
403					220	37	-084	032	51	-096		
404	6.0	7.0			280	60	-030	026	65	-147		
405 *	5.6	5.7			093	13	-090	273	77	-090		
406 H	4.7	4.7	<0.1		176	33	-114	024	60	-075		
501	6.1	7.4	30.0		260	50	-099	094	41	-080	8*m*	*P, SH*
502	5.2	5.3	0.2		253	67	-143	147	56	-027	6	*P, SH*
503	5.2	5.0	0.1		220	65	-139	111	54	-031	7	*P, SH*
504 H	5.4		0.1		336	25	-075	139	66	-097		
601	5.7		0.2		310	65	-140	201	54	-031	8	*P*
602	6.1		0.7		310	65	-124	186	41	-041	8	*P*
603	5.9	5.8	0.7		320	66	-140	212	54	-030		
604	6.2	6.9	30.0	+*F*	317	59	-085	127	31	-099	13*m*	*P, SH*
605 H	5.2	5.3	0.3		143	21	-072	304	70	-097		
606 H	5.5	5.8	0.8		174	31	-052	312	66	-110		
607 H	5.2	5.2	0.2		156	43	-076	317	49	-103		
711	6.0	6.6	15.0		200	58	-080	000	34	-106		
712 H	5.0	5.0	<0.1		094	38	-128	319	61	-065		
721	5.2	5.1			258	56	-112	115	40	-060		
731	5.5	6.2	1.1		303	74	-025	040	70	-165		
742		7.4			064	56	-090	244	34	-090		
743	5.5	5.3	0.2		188	61	-083	355	30	-101	14	*P, SH*

Table A2 *continued*

No.	m_b	M_s	M_o	f_p	s_1	d_1	r_1	s_2	d_2	r_2	dep	
744	5.9	6.0	4.2		090	74	-115	330	30	-034		
745	5.3	5.8	0.5		073	40	-140	312	68	-058		
746	5.6	6.3	2.3		252	66	-100	096	26*	-069		
747	5.8	6.6	9.1		098	60	-115	324	40	-052		
748	5.6	6.2	1.3		200	56	-040	315	58	-128	11	*P*
749	5.5		1.8		256	50	-090	076	40	-090		
750	5.8	6.3	3.1		090	74	-115	335	35	-030		
751 *	5.4	4.6			046	54	-090	226	36	-090	56	*pP*
752	5.7	5.7	0.6		277	49	-060	062	46	-115	6	*P*
753	5.3	4.8			283	56	-060	057	46	-126		
754	6.1	6.4	5.2	*+F*	278	46	-070	069	49	-110	6	*P,SH*
755	5.8	5.6			266	36	-105	104	56	-080		
756	5.2	5.3			284	56	-090	104	34*	-090		
757	5.9	6.7	6.8		285	40	-070	080	52	-107	12	*P,SH*
758	5.5	6.4	2.4	*+F*	250	42	-080	056	48	-100	7	*P,SH*
759	5.9	6.4	2.5	*+F*	068	47	-082	240	43	-095	4	*P,SH*
760 H	5.3	5.4	0.3		077	28	-121	291	66	-074		
761 H	5.1	4.9	0.1		212	38	-105	051	54	-079		
762 H	5.5	5.5	0.4		281	43	-072	077	50	-106		
763 H	5.4	5.3	0.1		256	33	-085	070	57	-093		
764	6.0	5.8	0.7	*+F*	201	47	-080	006	43	-101	5	*P,SH*
765 H	5.3	5.5	0.5		046	37	-155	295	75	-055		
782	5.2	6.4	2.7		268	70	-125	152	40	-032		
783	5.5	5.9	0.6		000	80	-090	180	10*	-090	12	*P*
784	6.0	6.8	18.0		302	36*	-090	122	54	-090		
785	5.3	5.7	0.8		101	70	-090	281	20*	-090		
786	5.6				340	40	-090	160	50	-090		
787	5.6	5.9	1.0		112	34*	-090	292	56	-090	8	*P*
788	5.5	6.0	1.7		090	40*	-104	290	52	-078	8	*P*
789	6.1	6.5	20.0	*+F*	281	34*	-090	101	56	-090	6*m*	*P*
790	5.5	5.6			101	50	-090	281	40	-090		
791	5.1	5.2			090	45	-090	270	45	-090		
792	6.0	7.2	88.0	*+F*	308	35	-090	128	55	-090	10*m*	*P*
793	5.2	4.9			077	33	-106	277	58	-080		
794	5.5	5.2	0.3		280	31	-100	115	59	-083	8	*P*
795	5.4	5.7	1.9		284	66	-090	104	24*	-090	8*m*	*P*
796	5.2	5.3	0.4		252	48	-102	090	44	-077		
797	5.5	6.0		*F*	064	50	-075	222	42	-107		
798	5.8	5.5	1.0		298	55	-077	095	37	-107	6	*P*
799	5.4	4.9			247	47	-126	114	54	-058		
800	5.7	6.7			041	60	-125	279	46	-043		
801 H	5.5	5.5	0.4		320	57	-039	074	58	-140		
901	6.0		8.5		256	50	-048	022	55	-128	29	*P*
902	5.3		0.1		047	40	-090	227	50	-090	17	*P*
903	5.5		0.3		008	60	-133	252	50	-040	7	*P*
904	5.7		0.3		335	50	-134	233	56	-050	27	*P*
905	5.9		0.2		000	50	-128	230	52	-053	13	*P*
906	5.9		1.0		120	63	-039	230	56	-148	6	*P*
907	5.7		0.2		345	50	-133	220	56	-052	25	*P*
908	5.2		0.1		168	63	-077	322	30	-115	14	*P*
909	5.2		0.2		348	56	-129	224	50	-046	12	*P*
910 H	5.1		0.1		158	35	-098	349	56	-084		
911 H	5.4	4.9	0.1		126	42	-122	347	56	-064		
912 H	5.4		0.1		215	13	-071	016	77	-094		
913			2.1		010	45	-090	190	45	-090	*m*	*P,SH*
914			4.5		010	45	-090	190	45	-090	*m*	*P,SH*
915 H	4.9		<0.1		211	45	-090	031	45	-090		
916 H	5.4	4.8	0.2		256	31	-045	029	68	-113		
917 H	5.2	5.4	0.6		318	22	-148	198	79	-071		
918 H	5.5	4.6	0.1		238	43	-084	050	48	-095		
919 H	4.9	4.8	0.1		168	37	-090	348	53	-090		
920 H	5.6	6.2	2.5		232	38	-051	007	61	-116		
1001	5.4	5.5	0.2		314	48	-106	158	45	-073	10	*P,SH*
1002	5.5	5.4	0.1		144	72	-124	030	38	-030	22	*P,SH*
1021	6.0	6.8	18.0		304	38	-085	117	52	-094	10	*P,SH*
1022	5.6	5.5	0.5		322	30	-080	131	60	-095	10	*P,SH*
1031	5.7	6.6			197	42	-034	313	68	-126		
1041	5.9	6.6	6.4	*+F*	225	45	-110	074	48	-071	8*m*	*P*
1051	6.0	6.0	3.0	*F*	220	49	-042	340	60	-130	7*m*	*P*
1061 H	5.5	5.1	0.3	*F*	015	34	-130	241	65	-066		
1071	6.4	6.2	3.5	*+F*	090	60	-147	340	62	-035	13	*P*
1081 H	5.0	4.8	0.2		156	21	-102	349	70	-086		
1091 H	5.3	4.7	0.1		081	38	-076	244	53	-100		

Table A3. References used for each earthquake, as numbered in the right-hand column of Table A1

REFERENCES

1. Wallace (1984)
2. Doser (1986)
3. Slemmons (1957)
4. Romney (1957)
5. Savage & Hastie (1966)
6. Myers & Hamilton (1964)
7. Doser (1985)
8. Westaway, R. *pers. comm.*
9. Smith & Sbar (1974)
10. Goff *et al.* (1987)
11. Langston & Butler (1976)
12. Bache *et al.* (1980)
13. Nabalek (in press)
14. Doser & Smith (1985)
15. Stein & Barrientos (1985)
16. Richens *et al.* (1987)
17. Zollweg & Richens (1985)
18. Chen & Molnar (1983)
19. Chen *et al.* (1981)
20. Tapponnier & Molnar (1977)
21. Huilan *et al.* (1983)
22. Vvedenskaya & Balakina (1960)
23. Tapponnier & Molnar (1979)
24. Nabalek *et al.* (1987)
25. Butler *et al.* (1979)
26. Westaway (1987)
27. Anderson & Jackson (1987)
28. Deschamps *et al.* (1984)
29. Westaway & Jackson (1987)
30. Deschamps & King (1983)
31. Gasparini *et al.* (1982)
32. Harvard Moment Tensor Solution
33. McKenzie (1978b)
34. H.J. Anderson & J.A.Jackson (unpub. data)
35. McKenzie (1972)
36. North (1977)
37. Shirokova (1972)
38. J.A. Jackson: replotted in crust from (35)
39. Fitch & Muirhead (1974)
40. Soufleris & Stewart (1981)
41. Jackson *et al.* (1982b)
42. Kim *et al.* (1984)
43. Jackson *et al.* (1982a)
44. Jackson & McKenzie (1984)
45. Eyidoğan (1983)
46. Stewart & Kanamori (1982)
47. Eyidoğan & Jackson (1985)
48. Shudofsky (1985)
49. Wagner & Langston (1986)
50. Grimison & Chen (1988)
51. Jemsek *et al.* (1986)
52. Jackson *et al.* (1988)
53. Huang & Solomon (1987)
54. McKenzie *et al.* (1970)
55. DSIR (1987)
56. Choy & Kind (1987)
57. Dorbath et al. (1984)
58. Lyon-Caen *et al.* (in press)
59. Anderson & Webb (in press)
60. Molnar & Deng (1984)